

1 Partitioning carbon sources between wetland and well-drained 2 ecosystems to a tropical first-order stream - Implications to carbon 3 cycling at the watershed scale (Nyong, Cameroon)

4 Moussa Moustapha¹, Loris Deirmendjian^{2, 3}, David Sebag^{4, 5, 6}, Jean-Jacques Braun^{2, 3, 7, 8}, Stéphane
5 Audry², Henriette Ateba Bessa⁷, Thierry Adatte⁹, Carole Causserand², Ibrahima Adamou¹, Benjamin
6 Ngounou Ngatcha¹, Frédéric Guérin^{2,3}.

7 ¹Université de Ngaoundéré, Faculté des Sciences, BP 454 Ngaoundéré, Cameroun

8 ²Géosciences Environnement Toulouse (GET- Université de Toulouse, CNRS, IRD), Université de Toulouse Paul Sabatier,
9 14 Avenue Edouard- Belin, 31400 Toulouse, France

10 ³IRD, UR 234, GET, 14 Avenue E. Belin, 31400, Toulouse, France

11 ⁴Normandie Univ, UNIROUEN, UNICAEN, CNRS, M2C, 76000 Rouen, France

12 ⁵HSM, IRD, CNRS, Université de Montpellier, Montpellier, France⁶IFPEN, Geosciences Dept, Rueil-Malmaison, France

13 ⁷Institut de Recherches Géologiques et Minières/Centre de Recherches Hydrologiques, BP 4110, Yaoundé, Cameroun

14 ⁸International Joint Laboratory DYCOFAC, IRGM-UY1-IRD, Rue Joseph Essono Balla, Quartier Elig Essono, BP 1857,
15 Yaoundé, Cameroun

16 ⁹Institut des Sciences de la Terre (ISTE), Université de Lausanne, GEOPOLIS, CH-1015 Lausanne, Switzerland

17 Correspondence to: Frédéric Guérin (frederic.guerin@ird.fr)

18 Abstract

19 Tropical rivers emit large amounts of carbon dioxide (CO₂) to the atmosphere, in particular due to large wetland to river carbon
20 (C) inputs. Yet, tropical African rivers remain largely understudied and little is known about the partitioning of C sources
21 between wetland and well-drained ecosystems to rivers. In a first-order sub-catchment (0.6 km²) of the Nyong watershed
22 (Cameroon 27 800 km²), we fortnightly measured C in all forms and ancillary parameters in groundwater in a well-drained
23 forest (hereafter referred as non-flooded forest groundwater) and in the stream. In a first-order sub-catchment (0.6 km²) of the
24 Nyong watershed (Cameroon, 27 800 km²), we fortnightly measured dissolved and particulate C in groundwater in a well-
25 drained forest (hereafter referred as non-flooded forest groundwater) and in the stream. In the first-order catchment, the simple
26 land use shared between wetland and well-drained forest, together with drainage data, allowed the partitioning of C sources
27 between wetland and well-drained ecosystems to the stream. Also, we fortnightly measured dissolved and particulate C
28 downstream the first-order stream to the main stem of order 6 and we supplemented C measurements with measures of
29 heterotrophic respiration in stream orders 1 and 5. In the first-order stream, dissolved organic and inorganic C and particulate
30 organic C (POC) concentrations increased during rainy seasons when the hydrological connectivity with the riparian wetland
31 increased whereas the concentrations of the same parameters decreased during dry seasons when the wetland was shrinking.
32 In larger streams (order > 1), the same seasonality was observed showing that wetland in headwaters were significant sources
33 of organic and inorganic C for downstream rivers, even though higher POC concentration evidenced an additional source of

POC in larger streams during rainy seasons that was most likely POC originating from floating macrophytes. During rainy seasons, the seasonal flush of organic matter from the wetland in the first order catchment and from the macrophytes in higher-order rivers significantly affected downstream metabolism, as evidenced by higher respiration rates in stream orders 5 ($756 \pm 333 \text{ gC-CO}_2 \text{ m}^{-2} \text{ yr}^{-1}$) compared to 1 ($286 \pm 228 \text{ gC-CO}_2 \text{ m}^{-2} \text{ yr}^{-1}$). In the first-order catchment, the sum of the C hydrologically exported from non-flooded forest groundwater ($6.2 \pm 3.0 \text{ MgC yr}^{-1}$) and wetland ($4.0 \pm 1.5 \text{ MgC yr}^{-1}$) to the stream represented 3-5% of the local catchment net C sink. In the first-order catchment, non-flooded forest groundwater exported 1.6 times more C than wetland, however, when weighed by surface area, C inputs from non-flooded forest groundwater and wetland to the stream contributed to 27% ($13.0 \pm 6.2 \text{ MgC yr}^{-1}$) and 73% ($33.0 \pm 12.4 \text{ MgC yr}^{-1}$) of the total hydrological C inputs, respectively. At the Nyong watershed scale, the yearly integrated CO_2 degassing from the entire river network was $652 \pm 161 \text{ GgC-CO}_2 \text{ yr}^{-1}$ ($23.4 \pm 5.8 \text{ MgC CO}_2 \text{ km}^{-2} \text{ yr}^{-1}$ when weighed by the Nyong watershed surface area) whereas average heterotrophic respiration in the river and CO_2 degassing rates were 521 ± 403 and $5\,085 \pm 2\,544 \text{ gC-CO}_2 \text{ m}^{-2} \text{ yr}^{-1}$, which implied that only ~10% of the CO_2 degassing at the water-air interface was supported by heterotrophic respiration in the river. In addition, the total fluvial C export to the ocean of $191 \pm 108 \text{ GgC yr}^{-1}$ ($10.3 \pm 5.8 \text{ MgC km}^{-2} \text{ yr}^{-1}$ when weighed by the Nyong watershed surface area) plus the yearly integrated CO_2 degassing from the entire river network represented ~11% of the net C sink estimated for the whole Nyong watershed. In tropical watershed, we show that wetlands largely influence riverine C variations and budget. Thus, ignoring the river–wetland connectivity might lead to the misrepresentation of C dynamics in tropical watershed.

1. Introduction

Despite their small surface area worldwide (Allen and Pavelsky, 2018), inland waters (rivers, lakes and reservoirs) have a critical role in the global carbon (C) cycle. Inland waters receive large amount of C from the drainage of land, i.e., from well-drained ecosystems as non-flooded soils and groundwater, and wetland, i.e., from flooded soils (Abril and Borges, 2019; Cole and Caraco, 2001). The C entering inland waters is processed and subsequently transferred to the atmosphere and the ocean (Cole et al., 2007; Ludwig et al., 1996; Meybeck, 1982; Tank et al., 2016). Besides, inland waters are significant hotspots of carbon dioxide (CO_2) degassing (e.g., Raymond et al., 2013) as they are usually supersaturated with CO_2 compared to the atmosphere. Since the seminal paper by Cole et al. (2007) who estimated that 0.75 PgC-CO_2 was emitted annually to the atmosphere from global inland waters, global emissions estimates have increased substantially. In the most spatially explicit scaling study, degassing estimate from global inland waters was $2.1 \text{ PgC-CO}_2 \text{ yr}^{-1}$ (Raymond et al., 2013). Later, this estimate has been updated with more accurate CO_2 emissions estimates from African and Amazonian rivers and from small ponds, resulting in the latest estimate of $3.9 \text{ PgC-CO}_2 \text{ yr}^{-1}$ to which $0.2\text{-}0.55 \text{ PgC-CO}_2 \text{ yr}^{-1}$ might be still added as CO_2 emissions estimates from rivers are usually not integrated over a full day (Borges et al., 2015a; Drake et al., 2018; Gómez-Gener et al., 2021; Holgerson and Raymond, 2016; Raymond et al., 2013; Sawakuchi et al., 2017). Globally, the latest estimate of

65 CO₂degassing from inland waters was in the same order of magnitude as the net terrestrial C sink (3.4 PgC yr⁻¹; Friedlingstein
66 et al., 2020).

67

68 Raymond et al. (2013) showed that CO₂ emissions from global rivers (1.8 PgC-CO₂ yr⁻¹) mainly depends on emissions in
69 tropical rivers, since tropical rivers account for ~80% of the global emissions. However, the magnitude of CO₂ emissions from
70 tropical rivers was poorly constrained because its estimation was based on very few data from the tropics and probably biased
71 by the overwhelming dominance of data from the Amazon basin over other tropical basins, resulting in uncertain interpolation
72 and scaling. Indeed, based on CO₂ emissions measurements in African and Amazonian rivers including the Amazon and the
73 Congo, Borges et al. (2015a) estimated that tropical rivers could emit alone 1.8±0.4 PgC-CO₂ yr⁻¹. This significant flux at the
74 global scale, estimated from direct measurements, demonstrates the importance of CO₂ emissions from tropical rivers, calling
75 for attention to tropical systems, in particular to Africa, where very few data on C stock and C cycle are available. These data
76 are crucial to refine the global CO₂ budget since tropical rivers have been identified in global earth modelling approaches as
77 systems exhibiting higher CO₂ emission rates per unit area than those in the temperate and boreal regions (Lauerwald et al.,
78 2015; Raymond et al., 2013). In addition, in these modelling studies the CO₂ emission upscaling was done using the GLORICH
79 dataset, in which the water CO₂ partial pressure (pCO₂) is actually estimated from pH and total alkalinity (TA). This calculation
80 method leads to overestimate pCO₂ up to 75 times, notably in low buffered and high organic waters, that are representative for
81 boreal and tropical rivers (Abril et al., 2015). In contrast, pCO₂ estimated from pH and dissolved inorganic C (DIC)
82 measurements is relatively robust (Åberg and Wallin, 2014). Thus, empirically measuring pCO₂ and to a lesser extent DIC,
83 rather than relying on pCO₂ estimated from pH and TA that is prone to large error, are key to improving CO₂ emissions
84 estimates from inland waters.

85

86 In tropical watersheds, CO₂-enriched wetland waters directly contribute to the CO₂ dissolved in riverine waters, in particular
87 during high water periods when wetland-river connectivity is increasing (Abril et al., 2014; Borges et al., 2015a, 2015b, 2019).
88 Indeed, tropical wetlands are productivity hotspots and a large fraction of their biomass is released to the water through litter-
89 fall and roots exudation, which fuels heterotrophic respiration in the wetland and enrich the water in CO₂ (Abril et al., 2014;
90 Abril and Borges, 2019). In addition, during high water periods, the drainage of tropical wetlands releases large amounts of C
91 and organic matter (OM) to the rivers that might enhance heterotrophic respiration in downstream rivers, indirectly increasing
92 CO₂ concentration in tropical rivers (Borges et al., 2019; Engle et al., 2008; Lambert et al., 2016a; Richey et al., 2002).
93 Nonetheless, in large tropical rivers, heterotrophic respiration in the river is usually a small component of the riverine CO₂
94 budget because of the large dominance of the drainage of wetland in the overall budget (Abril et al., 2014; Borges et al., 2019).
95 Large tropical rivers have the ability to transport CO₂-enriched wetland waters far enough from the point source because of
96 faster water movement relative to gas exchange (Abril et al., 2014). In the Amazon and the Congo watersheds, the intensity of
97 the CO₂ degassing from the rivers has been thus related to the percentage of the wetland cover (Abril et al., 2014; Borges et
98 al., 2019, 2015b), showing that wetlands are the main source of OM fuelling CO₂ production in tropical watersheds. However,

99 as in temperate rivers, the CO₂ dissolved in tropical rivers also originates from well-drained ecosystems (non-flooded soils and
100 groundwater) in which CO₂ comes from plant root and microbial respiration (Johnson et al., 2006, 2008).
101

102 In tropical watersheds, considering the importance of lateral inputs in sustaining riverine C fluxes, quantifying hydrological C
103 fluxes resulting from the drainage of well-drained ecosystems and wetlands is thus fundamental to close the riverine C budget.
104 Still, in tropical watersheds, questions remain about the quantification and partitioning of hydrological C fluxes resulting from
105 the drainage of well-drained ecosystems and wetland and their significance in comparison to the local net terrestrial C sink
106 (Duvert et al., 2020a). At the plot scale and in temperate climate, the very few studies that compare the local net terrestrial C
107 sink with direct measurements of the hydrological export of C from well-drained ecosystems showed less than 3% of the local
108 net terrestrial C sink is actually exported to the aquatic environment (Deirmendjian et al., 2018; Kindler et al., 2011). In a small
109 tropical catchment (140 km²) in Australia, in which the land use was shared between dry savanna and wetland, the contribution
110 of the total hydrological export of C to the stream relative to the local net terrestrial C sink was 7% (Duvert et al., 2020a).
111 However, Duvert et al. (2020a) did not partition the hydrological export of C to the river between dry savanna and wetland.
112 Furthermore, to the best of our knowledge, partitioning the hydrological export of C to rivers between well-drained ecosystems
113 and wetland has never been done in tropical Africa. As the warmer and wetter conditions expected in tropical Africa in a near
114 future will likely modify C fluxes at the watershed scale, integrative studies on C cycling in tropical watersheds are required
115 to get a better grasp of the present drivers of riverine CO₂ emissions and thus to better predict future changes (Duvert et al.,
116 2020a).
117

118 The Nyong River basin (South Cameroon) belongs to the Critical Zone Observatories' (CZO; Gaillardet et al., 2018) network
119 named Multiscale TROPical CatchmentS (M-TROPICS; Audry et al., 2021) and is a long-term monitoring program of
120 hydrological and environmental parameters in the tropics. In this study, we used rainfall, water table level and river discharges
121 measured in the framework of the M-TROPICS observatory. The first objective of this study is to estimate the riverine C
122 budget of a first-order catchment, the Mengong catchment, a nested sub-catchment of the Nyong watershed. The hydrological
123 inputs of C from the drainage of land (i.e., from groundwater in a well-drained forest; hereafter referred as non-flooded forest
124 groundwater) and from wetland to the stream, the heterotrophic respiration in the river, the CO₂ degassed to the atmosphere,
125 and the C hydrologically exported at the stream outlet are estimated and compared with the local net terrestrial C sink, and
126 will be discussed. In line with recent studies in large tropical watersheds (Abril et al., 2014; Borges et al., 2015; 2019), we
127 expect that lateral inputs of C from wetland to the stream are significant in comparison with lateral inputs of C from non-
128 flooded forest groundwater. The second objective of this study is to evaluate the changes in organic and inorganic C
129 concentration over the seasons in the riverine continuum, from non-flooded forest groundwater to the different stream orders
130 (order 1 to 6). In the Nyong watershed, downstream (order > 1) riverine C concentrations throughout a water cycle will be
131 compared with those observed upstream in the Mengong stream (order 1) in order to evaluate how the biogeochemical cycle
132 of C and its resulting atmospheric CO₂ emissions is affected by the connectivity with the wetland domain.

133 **2. Materials and Methods**

134 **2.1. Study site**

135 **2.1.1. The Nyong watershed**

136 The Nyong watershed (27 800 km², Cameroon) is located between 2.8 and 4.5° N and 9.5 and 13.3° E, mainly in the Southern
137 Cameroon Plateau (600-900 m high) (Fig. 1). The landscape of the Southern Cameroon Plateau mostly consists in a succession
138 of convex rounded hills separated by flat wetlands of variable sizes (Olivry, 1986). We adopt the common definition of
139 wetlands as habitats with continuous, seasonal, or periodic standing water or saturated soils (Mitsch et al., 2012). The main
140 stem (the Nyong River, stream order 6) is 690 km long and flows west to the Atlantic Ocean (Fig.1). In the eastern part of the
141 watershed (from Abong Mbang to Akonolinga; Fig. 1), the Nyong River flows through large riparian wetlands of variable size
142 that laterally extended from the river up to 2-3 km according to seasons (Olivry, 1986). In the western part of the basin
143 (downstream to Akonolinga; Fig. 1), riparian wetlands extent is less pronounced and the Nyong river flows through mature
144 forest in a well-channelled river bed (Olivry, 1986).

145
146 The Nyong watershed experiences an equatorial climate with four seasons with two maxima and minima: a short rainy season
147 (SRS: Apr-June), a short dry season (SDS: July-August), a long rainy season (LRS: Sept.-Nov) and a long dry season (LDS:
148 Dec-March) (Suchel, 1987). The catchment lithology is composed of metamorphic and plutonic rocks with the absence of
149 carbonate rocks and minerals (Viers et al., 2000). Slopes and hills are recovered by a thick lateritic profile (20-40 m) poor in
150 C, whereas in the wetlands (i.e., in the depressions) the upper part of the hydromorphic soils shows an enrichment in OM
151 (Boeglin et al., 2003; Nyeck et al., 1999). Ferrealitic soils covers about 80% of the Nyong watershed, and this soil cover can
152 reach 40 m thick (Braun et al., 2005). On hills and hillsides, the vegetation cover is dominated by semi deciduous-forest
153 whereas in the wetlands Raffia palm trees usually dominates.

154
155 In the Nyong watershed, six sites were sampling fortnightly from January to December 2016 (22 times during the sampling
156 period), namely from upstream to downstream: the small first-order Mengong catchment (at the source and the outlet of the
157 catchment), the Awout River (order 3), the So'o River (order 4), and the Nyong River at Mbalmayo (order 5) and Olama (order
158 6); all sampling sites were located in the western part of the watershed (Table 1; Fig. 1). Noteworthy, the Mengong catchment
159 is described in detail in the next section 2.1.2. The Awout River flows for about 30 km in a partially marshy river bed. The
160 So'o River is the southern forest extension of the Nyong Watershed and is the main tributary on the left bank of the Nyong
161 River. The Mbalmayo sampling station is located on the Nyong River upstream the confluence with the So'o, while the Olama
162 sampling station is located downstream the confluence with the So'o. Each sampling site (except the Mengong source) are
163 gauging stations calibrated for discharges measurements, monitored daily since 1998 and are publicly available at
164 <https://doi.org/10.6096/BVET.CMR.HYDRO> (Audry et al., 2021). The yearly average discharge of the Nyong River at Olama

165 was $\sim 195 \text{ m}^3 \text{ s}^{-1}$ for both the 1998-2020 period (long-term average) and the year of sampling 2016 (Fig. 2). Also, the average
166 monthly discharges during the year 2016 did not differ significantly from the average monthly discharges from the 1998-2020
167 period (Fig. 2). The annual rainfall in the Nyong watershed was 1986 mm in 2016 which is in the upper range of rainfall
168 ($1600 \pm 290 \text{ mm}$) for the 1998-2020 period (Fig. 2). Altogether, this shows that hydrological fluxes occurring during the
169 sampling year 2016 were typical of the hydrological fluxes usually occurring in the Nyong watershed.

170

171 In addition, the C exported at the most downstream station (Nyong River at Olama) is considered as representative as the C
172 exported to the Atlantic Ocean by the whole Nyong watershed because the contribution of the tributaries downstream from
173 this station is negligible (Nkoue-ndondo, 2008). Indeed, Brunet et al. (2009) measured both hydrological export of DIC and
174 DOC from the Nyong River at Olama and also more downstream near Déhané (very close to the Nyong river outlet; Fig. 1)
175 and they showed that these fluxes (in $\text{MgC km}^{-2} \text{ yr}^{-1}$, weighed by the catchment surface area drained at Olama or Edea) were
176 similar at Olama (4.2 ± 0.1 and $0.8 \pm 0.1 \text{ MgC km}^{-2} \text{ yr}^{-1}$, for DOC and DIC, respectively) and Déhané (3.9 ± 0.2 and $1.1 \pm 0.1 \text{ MgC}$
177 $\text{km}^{-2} \text{ yr}^{-1}$).

178 2.1.2. The first-order Mengong catchment

179 The Mengong Catchment is 0.6 km^2 and consists of a convexo-concave landscape, ranging from 669 m at the river outlet to
180 703 m at the top of the hill, separated by a flat wetland that covers 0.12 km^2 (Fig. 3). Semi-deciduous rainforest (*Sterculiaceae*-
181 *Ulmaceae*, C3 plant) covers most of the hills and hillsides, whereas most of the wetland vegetation comprises semi-aquatic
182 plants of the Araceae family (C4) and tree populations of Gilbertiodendron deweveri (*Caesalpinaceae*, C3) and Raffia
183 monbuttorum (raffia palm trees, C3) (Braun et al., 2005, 2012). The hillside soil cover is a thick lateritic soil that consists of a
184 succession of four main horizons, namely from the bottom to the top, the saprolitic horizon, the mottled clay horizon, the
185 ferruginous horizon, and the soft clayey topsoil; the thickness and distribution of these soil layers depend on the topographic
186 position (Fig. S1). The groundwater floods the fractured bedrock, the entire saprolite, and partly the mottled clay horizon
187 (Braun et al. 2005; Fig. 3). The soil cover is 15 m thick at the top of the north hill (piezometer 1); the depth however, decreases
188 progressively towards the flat wetland (Fig. 3). The roots of the hillside vegetation are essentially located in the topsoil horizon,
189 which has a depth of 5 to 6 m at the top of the hill (at piezometer 1) and has a depth of 3 to 4 m (at piezometer 2) at the mid-
190 slope (Braun et al. 2005; Fig. 3). In the wetland, a dark-brown organic-rich sandy material with a thickness ranging from 0.1
191 to 1 m tops the hydromorphic soil. In this organic horizon, OM can reach up to 20% by weight, and it is composed of a thick
192 mat of dead and living roots and tubers originating from the wetland vegetation (Braun et al. 2005; Fig. 3). Noteworthy, the
193 first-order Mengong catchment is considered representative of the South Cameroon plateau (and thus of the Nyong watershed)
194 that also consists itself in multiconvex land form developed on granitic terrains separated by flat wetland (Braun et al., 2012).
195 Moreover, the same soil cover and plant species are observed in the Mengong catchment and in the Nyong watershed but it
196 should be noted that the wetland extent is larger in the Mengong Catchment (20%) than in the whole watershed ($\sim 5\%$) (Table.

197 1). Note that wetland extent in larger catchment was estimated from GIS analysis using the global wetland map by Gumbricht
198 et al. (2017) (Table 1).

199
200 Groundwater draining the hillside emerges at two sources (Q_{hill}) in the catchment head and at specific seepage points (Q_{base})
201 along the hillside/wetland boundaries (Fig. 3). Only one of these two sources is perennial, the other dries up during dry periods
202 (Fig. 3; Braun et al., 2005; Maréchal et al., 2011). Note that groundwater that emerges at sources and at specific seepage points
203 will be further referred as non-flooded forest groundwater. Q_{hill} is conveyed to the stream with negligible interaction with the
204 wetland, while Q_{base} fed the wetland, which is flooded all year long (Maréchal et al., 2011). In addition, according to
205 observations made in the Mengong catchment during most of the rainfall events by Maréchal et al. (2011), it is assumed that
206 the overland flow can be neglected on the forested hillside as the porous soil have a high infiltration capacity. Therefore, the
207 water budget of the hillside aquifer system, as shown in Fig. 3, is the following:

$$208 \quad R_{hill} = Q_{hill} + Q_{base} \quad (Eq. 1)$$

209 where,

210 R_{hill} is the recharge rate of the hillside by infiltration of rain water. Maréchal et al. (2011) estimated R_{hill} at 20% of the yearly
211 rainfall occurring in the Mengong catchment, based on a hydrological model related to chloride mass balance at the catchment
212 scale. Q_{hill} and Q_{base} represents 90 and 10% of R_{hill} , respectively.

213
214 The total streamflow at the outlet of the Mengong catchment (Q_{ST}), as shown in Fig. 3, is the sum of the contributions of Q_{hill} ,
215 the exchange flow between the wetland and the stream ($Q_{WL/ST}$) and the overland flow on the wetland surface (OF_{WL}), as the
216 following:

$$217 \quad Q_{ST} = Q_{hill} + Q_{WL/ST} + OF_{WL} \quad (Eq. 2)$$

218 where,

219 OF_{WL} represents 35% of the of the yearly rainfall in the Mengong catchment (Maréchal et al. 2011). Note that both Q_{hill} and
220 OF_{WL} can be estimated from the yearly rainfall over the Mengong catchment and Q_{ST} is measured. $Q_{WL/ST}$ can be thus obtained
221 by difference, but only on a yearly basis.

222 2.2. Sampling and laboratory work

223 The water samples in the Nyong, So'o and Awout Rivers were collected from bridges using a Niskin Bottle (3L) attached to a
224 rope. At the Mengong source, the water samples were taken directly from the source where non-flooded forest groundwater
225 seeps out from a polyvinyl chloride pipe. Note that the pipe is only a few centimetres long, thus limiting considerably the
226 contact time between water and atmospheric air. Additionally, each sampling bottle was left to overflow to avoid catching air
227 bubbles. At the Mengong outlet, the shallow depth permitted retrieving water samples directly from the stream.

228

229 Dissolved inorganic C (DIC), TA, dissolved and particulate organic C (DOC and POC), total suspended matter (TSM) and the
230 POC content of the TSM (POC%) were measured from single samples. At each sampling site, we measured the physico-
231 chemical parameters (temperature, pH, oxygen saturation, and specific conductivity). The water temperature, pH, oxygen
232 saturation and specific conductivity were measured *in-situ* using portable probes (WTW®) between January and March 2016
233 and using an YSI® ProDSS Multiparameter Digital Water Quality Meter between April and December 2016. Calibration of
234 sensors was carried out prior to sampling campaigns and regularly checked during the campaigns. For the WTW® probes, the
235 conductivity cell was calibrated with a 1 000 $\mu\text{S cm}^{-1}$ (25°C) standard and the pH probe was calibrated using NBS buffer
236 solutions (4 and 7). The YSI® ProDSS was calibrated using the protocols recommended by the manufacturer. The conditioning
237 of water samples was done directly after the field trips in Cameroon at the Institut de Recherches Géologiques et Minières
238 (IRGM) of Yaounde, while chemical analyses were done in France at Toulouse in the laboratory of Géosciences Et
239 Environnement (GET). For TSM, POC and POC%, a filtration (0.5-1.5 L) was carried out on pre-weighed and pre-combusted
240 GF/F glass fibre filters (porosity of 0.7 μm). The filters were then dried at 60 °C and stored in the dark at room temperature
241 for subsequent analysis. TSM was determined by gravimetry with a Sartorius scale (precision of the scale was ± 0.1 mg). The
242 filters were acidified in crucibles with 2N HCl to remove carbonates and were then dried at 60 °C to remove inorganic C and
243 the remaining acid and water and then analysed by the Rock Eval pyrolysis method to measure POC and POC% (Lafargue et
244 al., 1998). For DOC, a portion of the POC filtrate was kept in glass bottles (60 mL) pyrolyzed beforehand, in which 3 drops
245 of phosphoric acid (85% H_3PO_4) were added to convert all DIC species to CO_2 . The glass bottles were sealed with septa made
246 of polytetrafluoroethylene (PTFE). DOC samples were stored at 3-5°C and DOC concentrations were measured by thermal
247 oxidation after a DIC removal step with a SHIMADZU TOC 500 analyser in TOC-IC mode (Sharp, 1993).

248

249 We stored TA samples at 20°C in polypropylene bottles after filtration using a syringe equipped with acetate cellulose filters
250 (porosity of 0.22 μm). TA was then analysed by automated electro-titration (Titrino Metrohm®) on 50 mL-samples with 0.1
251 N HCl as the titrant. The equivalence point was determined from pH between 4 and 3 with the Gran method (Gran, 1952). DIC
252 samples were collected in 70 mL glass serum bottles sealed with a butyl stopper and treated with 0.3 mL of HgCl_2 at 20 g L^{-1}
253 to avoid microbial respiration during storage. Vials were carefully sealed such that no air remained in contact with samples
254 and were stored in the dark to prevent photo-oxidation. DIC was measured with the headspace technique. The headspace was
255 created with 15 mL of N_2 gas, and 100 μL of 85% H_3PO_4 was added in the serum bottles to convert all DIC species to CO_2 .
256 After strong shaking and overnight equilibration at constant room temperature, a subsample of the headspace (1 mL) was
257 injected with a gastight syringe into a gas chromatograph equipped with a flame ionization detector (SRI 8610C GC-FID). The
258 gas chromatograph was calibrated with CO_2 standards of 400, 1 000 and 3 000 ppm (Air Liquide® France). In addition, we
259 estimated the water pCO_2 from the CO_2SYS software (Lewis and Wallace Upton, 1998), using DIC, pH, water temperature
260 measurements, and the carbonic acid dissociation constants of Millero (1979) and the CO_2 solubility from Weiss (1974).

261

In addition, we carried out 14 measurements of heterotrophic respiration in the river at two sampling sites (in the Mengong stream and in the Nyong River at Mbalmayo). For each sampling, six 70-mL serum bottles collected similarly as for DIC samples, were used for the determination of heterotrophic respiration in the river. Three serum bottles were directly poisoned in the field with 0.3 mL of HgCl_2 at 20 g L^{-1} . The three other serum bottles were incubated in a cool-dark box during 24 hours. The cool-dark box was protected from light and filled with water from the river to maintain inside the cool-dark box a water temperature similar to the water temperature observed in the river. At the end of the incubations, the serum bottles were poisoned with 0.3 mL of HgCl_2 and stored in the dark and at room temperature. To estimate volumetric rates of heterotrophic respiration in the river, we measured the increase in CO_2 in the incubated serum bottles compared to those poisoned directly in the field. CO_2 was measured similarly as for DIC, using the headspace technique but without a prior acidification with H_3PO_4 . Subsequently, volumetric rates of heterotrophic respiration in the river were depth-integrated with the river depth at the day of sampling. The river depth was retrieved from discharge-depth relationship established in the framework of the M-TROPICS observatory. Noteworthy, our method does not represent total heterotrophic respiration in the river since it does not include benthic respiration. A mean benthic respiration measured in various tropical rivers of $222 \text{ gC m}^{-2} \text{ yr}^{-1}$ by Cardoso et al. (2014) was therefore added to estimate total heterotrophic respiration in the river.

2.3. Determination of catchments surface area, water surface area, slope and gas transfer velocity (k_{600})

In the Nyong watershed, the sub-catchment surface areas and the determination of the different stream orders were estimated from the hydrological modelling tools available in QGIS3.16® and the digital elevation model (DEM, 15 sec resolution) conditioned for hydrology (HydroSHEDS; Lehner et al., 2008). In the Nyong watershed, the HydroSHEDS flowline dataset (15 sec resolution) enabled the precise determination of the total length of each stream order (1 to 6). To estimate the average monthly river width (W) in each stream order of the Nyong watershed, we used the average monthly discharges from the five gauging stations (located on stream-orders 1, 3, 4, 5 and 6) and the hydraulic equation described by Raymond et al. (2012), as follows:

$$W = 12.88Q_{\text{monthly}}^{0.42} \quad (\text{Eq. 3})$$

where,

Q_{monthly} is the average monthly discharge in 2016 in the stream orders 1, 3, 4, 5 or 6.

Since we did not measure discharge in stream order 2, the average width of stream order 2 was extrapolated from the best exponential regression curve from the relationship between stream order and average monthly river width, as indeed, river width within a basin scale exponentially with stream order for all river orders (Strahler, 1957). We used the average monthly river width and the total length per stream order to estimate the monthly water surface area per stream order. We fused the HydroSHEDS DEM and flowline dataset to assign an altitude to each river point and thus to determine the average slope (S) per stream order. To calculate the average monthly flow velocity (V) per stream order, we used the following hydraulic equation described by Raymond et al. (2012), as follows:

$$V = 0.19Q_{\text{monthly}}^{0.29} \quad (\text{Eq. 4})$$

295 The average monthly flow velocity in stream order 2 was extrapolated from the best exponential regression curve from the
 296 relationship between stream order and monthly average flow velocity. In each stream order, the monthly gas transfer velocity
 297 normalized to a Schmidt number of 600 (k_{600} in m d^{-1}) was derived from the parameterization as a function of S (unitless) and
 298 V (m s^{-1}) as in the Eq. 5 by Raymond et al. (2012):

$$299 \quad k_{600} = VS*2841+2.02 \quad (\text{Eq. 5})$$

300 As described by Borges et al. (2019), we chose this parameterization because it is based on the most comprehensive
 301 compilation of k values in streams which, in addition, was used in the global upscaling of CO_2 emissions from rivers by both
 302 Raymond et al. (2013) and Lauerwald et al. (2015).

303 **2.4. C fluxes at the Nyong watershed scale**

304 **2.4.1. CO_2 degassing and heterotrophic respiration**

305 In each stream order, monthly rate of CO_2 degassing at the water-air interface (F_{degas} ; in $\text{gC-CO}_2 \text{ m}^{-2} \text{ yr}^{-1}$) was estimated as
 306 follows:

$$307 \quad F_{\text{degas}} = k_{600} K_0 (p\text{CO}_{2w} - p\text{CO}_{2a}) \quad (\text{Eq. 6})$$

308 where,

309 K_0 is the solubility coefficient of CO_2 determined from the water temperature (Weiss, 1974), k_{600} is the monthly gas transfer
 310 velocity of CO_2 (section 2.3), $p\text{CO}_{2w}$ and $p\text{CO}_{2a}$ are the monthly partial pressures of CO_2 in the surface waters of the different
 311 stream orders and in the atmosphere (set to 400 ppmv), respectively.

312

313 In each stream order, we multiplied monthly F_{degas} in $\text{gC-CO}_2 \text{ m}^{-2} \text{ yr}^{-1}$ by the respective monthly water surface area to estimate
 314 the monthly CO_2 emissions (F_{degas} in $\text{GgC-CO}_2 \text{ yr}^{-1}$) integrated in each stream order. We summed F_{degas} in $\text{GgC-CO}_2 \text{ yr}^{-1}$ in
 315 each stream order to estimate the total quantity of CO_2 degassed from the Nyong watershed from the entire river network and
 316 then normalized by the Nyong watershed surface area ($\text{MgC-CO}_2 \text{ km}^{-2} \text{ yr}^{-1}$). Note, we did not measure $p\text{CO}_2$ in second-order
 317 streams but estimated the $p\text{CO}_2$ by averaging the $p\text{CO}_2$ measured in the first- and third-order streams.

318

319 At the watershed scale, volumetric rates of heterotrophic respiration in the river were estimated from the increase in CO_2 in
 320 the incubated serum bottles over 24h in stream orders 1 and 5. The volumetric respiration rates in stream orders 1 and 5 were
 321 depth-integrated and subsequently averaged to estimate an average rate of heterotrophic respiration from the entire river
 322 network of the Nyong watershed.

323 **2.4.2. C export to the ocean**

324 The C hydrologically exported to the ocean (F_{ocean}) was calculated monthly at the most downstream station (Nyong at Olama)
 325 as the following:

326 $F_{\text{ocean}} = Q_{\text{olama}} [C]_{\text{olama}}$ (Eq. 7)
 327 where Q_{olama} and $[C]_{\text{olama}}$ are the monthly average discharges and concentrations of POC, DIC or DOC at Olama, respectively.
 328 F_{ocean} was estimated in GgC yr^{-1} and then normalized by the catchment surface area at Olama ($\text{MgC km}^{-2} \text{yr}^{-1}$).

329 **2.5. Stream C budget of the first-order Mengong catchment**

330 **2.5.1. The different C fluxes**

331 At the Mengong catchment scale, as described above in the section 2.1.2, there are two sources fuelling the Mengong stream
 332 with C, namely non-flooded forest groundwater (F_{GW}) and wetland (F_{WL}). The C entering the Mengong stream has two outputs
 333 as this C is either degassed at the water-air interface in the form of CO_2 (F_{D}) or hydrologically exported at the stream outlet
 334 (F_{OUT}). Noteworthy, heterotrophic respiration in the stream (F_{RH}) is considered as an C input for the DIC budget, while a C
 335 output for the DOC budget (assuming respiration occurs on DOC only). At the Mengong catchment scale, riverine DIC, DOC
 336 and POC budgets ($\text{DIC}_{\text{budget}}$, $\text{DOC}_{\text{budget}}$, $\text{POC}_{\text{budget}}$) are thus the difference between C inputs and outputs, as follows:

$$337 \text{DIC}_{\text{budget}} = F_{\text{GW}} + F_{\text{WL}} + F_{\text{RH}} - F_{\text{D}} - F_{\text{OUT}} \quad (\text{Eq. 8})$$

$$338 \text{DOC}_{\text{budget}} = F_{\text{GW}} + F_{\text{WL}} - F_{\text{RH}} - F_{\text{OUT}} \quad (\text{Eq. 9})$$

$$339 \text{POC}_{\text{budget}} = F_{\text{WL}} - F_{\text{OUT}} \quad (\text{Eq. 10})$$

340 Noteworthy, $\text{DIC}_{\text{budget}}$, $\text{DOC}_{\text{budget}}$ and $\text{POC}_{\text{budget}}$ cannot be estimated monthly as for F_{degas} or F_{ocean} at the Nyong watershed
 341 scale, because water fluxes described in Equations 1 and 2, in particular Q_{hill} and OF_{WL} , which are needed to estimate F_{GW} and
 342 F_{WL} (see section 2.5.2), can only be estimated yearly from yearly rainfall in the Mengong catchment (see section 2.1.2).

343 **2.5.2. Hydrological C inputs to the stream from non-flooded forest groundwater and wetland**

344 According to equations 1 and 2, the quantity of dissolved carbon leached from non-flooded forest groundwater to the Mengong
 345 stream (F_{GW}) was estimated as the following:

$$346 F_{\text{GW}} = Q_{\text{hill}} [C]_{\text{GW}} \quad (\text{Eq. 11})$$

347 where,

348 $[C]_{\text{GW}}$ is the yearly average concentration of DIC or DOC in the Mengong source. F_{GW} (MgC yr^{-1}) was normalized by the
 349 surface area of 0.48 km^2 drained by the hillside ($\text{MgC km}^{-2} \text{yr}^{-1}$). Noteworthy, F_{GW} represents hydrological input of C to the
 350 stream from the drainage of land (well-drained ecosystem).

351

352 A part of non-flooded forest groundwater fed the wetland ($F_{\text{GW-bis}}$) and can be estimated as the following:

$$353 F_{\text{GW-bis}} = Q_{\text{base}} [C]_{\text{GW}} \quad (\text{Eq. 12})$$

354 $F_{\text{GW-bis}}$ does not account to the stream C budget because Q_{base} is not feeding the stream, but does account to the total quantity
 355 of C hydrologically leached from land. $F_{\text{GW-bis}}$ (MgC yr^{-1}) was normalized by the surface area drained by the hillside (MgC
 356 $\text{km}^{-2} \text{yr}^{-1}$).

357

358 According to equations 1 and 2, the quantity of dissolved C leached from the wetland to the Mengong stream (F_{WL}) was
359 estimated as the following:

360
$$F_{WL} = (OF_{WL} + Q_{WL/ST}) * [C]_{WL} \quad (Eq. 13)$$

361 where,

362 $[C]_{WL}$ are the concentrations of DOC or DIC in the topsoil solution (0.4 m) of the Mengong wetland, measured at 1420 ± 750
363 and $1430 \pm 900 \mu\text{mol L}^{-1}$ by Braun et al. (2005) and Nkoue Ndondo et al. (2020), respectively. F_{WL} (MgC yr^{-1}) was normalized
364 by the surface area of 0.12 km^2 drained by the wetland ($\text{MgC km}^{-2} \text{ yr}^{-1}$).

365

366 In the Mengong catchment, as described in the section 2.1.2, overland flow on hillsides is negligible and there is no particulate
367 C in non-flooded forest groundwater. Therefore, it can be safely assumed that POC at the Mengong outlet should originates
368 mostly from the drainage and erosion of the wetland. Accordingly, it was assumed that the hydrological export of POC at the
369 Mengong outlet is similar to the POC hydrologically exported from the wetland (F_{WL}). For POC, F_{WL} can thus be estimated as
370 the following:

371
$$F_{WL} = Q_{\text{outlet}} [POC]_{\text{OUT}} \quad (Eq. 14)$$

372 where,

373 Q_{outlet} and $[POC]_{\text{OUT}}$ are the yearly average discharge and POC concentration at the Mengong outlet, respectively. F_{WL} (MgC
374 yr^{-1}) was normalized by the surface area of the wetland ($\text{MgC km}^{-2} \text{ yr}^{-1}$).

375 **2.5.3. CO₂ degassing and heterotrophic respiration in the stream**

376 It has been shown that a large fraction of CO₂ degassing in headwaters was actually missed by conventional stream sampling
377 because a large fraction of the degassing occurs as hotspots in the vicinity of groundwater resurgences (e.g., Deirmendjian and
378 Abril, 2018; Johnson et al., 2008). Therefore, F_D ($\text{MgC-CO}_2 \text{ yr}^{-1}$) was estimated from a mass balance that calculates the loss
379 of the dissolved CO₂ between non-flooded forest groundwater (F_{D-GW}) (or wetland; F_{D-WL}) and stream water, using CO₂
380 concentrations and drainage data, a method similar to Deirmendjian and Abril (2018) and Duvert et al. (2020a), as the
381 following:

382
$$F_{D-GW} = ([CO_2]_{GW} - [CO_2]_{OUT}) * Q_{Hill} \quad (Eq. 15)$$

383
$$F_{D-WL} = ([CO_2]_{WL} - [CO_2]_{OUT}) * (OF_{WL} + Q_{WL/ST}) \quad (Eq. 16)$$

384
$$F_D = F_{D-GW} + F_{D-WL} \quad (Eq. 17)$$

385 where,

386 $[CO_2]_{GW}$, $[CO_2]_{WL}$ and $[CO_2]_{OUT}$ are the yearly average CO₂ concentrations in non-flooded forest groundwater, wetland, and
387 stream outlet, respectively. F_D , F_{D-GW} and F_{D-WL} (all three fluxes in $\text{MgC-CO}_2 \text{ yr}^{-1}$) were then normalized by the surface area
388 of the Mengong catchment ($\text{MgC-CO}_2 \text{ km}^{-2} \text{ yr}^{-1}$), the surface area drained by the hillside ($\text{MgC-CO}_2 \text{ km}^{-2} \text{ yr}^{-1}$), and the surface
389 area drained by the wetland ($\text{MgC-CO}_2 \text{ km}^{-2} \text{ yr}^{-1}$), respectively.

390

391 Rates of heterotrophic respiration in the Mengong stream were estimated from the increase in CO₂ in the incubated serum
392 bottles over 24h in the Mengong stream, which were subsequently depth-integrated. In the Mengong catchment, depth-
393 integrated rates of heterotrophic respiration in the river were multiplied by the Mengong stream surface area to obtain the
394 integrated contribution of heterotrophic respiration for the whole stream (F_{RH} in MgC-CO₂ yr⁻¹). To estimate the Mengong
395 stream surface area, stream width was estimated from equation 3 whereas stream length (750 m) was empirically determined
396 from field measurement by Maréchal et al. (2011). F_{RH} was then normalized by the surface area of the Mengong catchment
397 (MgC-CO₂ km⁻² yr⁻¹).

398 **2.5.4. C hydrologically exported at the Mengong stream outlet**

399 Based on equation 2, the quantity of C hydrologically exported at the outlet of the Mengong catchment (MgC yr⁻¹) can be
400 estimated as the following:

401
$$F_{OUT} = Q_{ST} [C]_{OUT} \quad (Eq. 18)$$

402 where, [C]_{OUT} is the concentration of POC, DOC or DIC at the Mengong stream outlet, respectively. F_{OUT} (MgC yr⁻¹) was then
403 normalized by the surface area of the wetland (MgC km⁻² yr⁻¹).

404 **3. Results**

405 **3.1. Hydrology**

406 In 2016, the discharges were 0.009±0.002 (range was 0-0.35), 3.9±4.8 (0-35), 35.6±40.6 (3.4-175), 146±112 (21-392) and
407 195±160 (8-640) m³ s⁻¹, in stream orders, 1, 3, 4, 5 and 6, respectively (Table 1, Fig. 2). All river discharges seasonally peaked
408 twice a year during the two rainy seasons, both separated by dry seasons; the groundwater water table followed the same trend
409 (Figs. 2, 4-5). Specifically, the beginning to middle of the rainy seasons corresponded to a period of increasing river discharge
410 and groundwater water table level, while the end of the rainy seasons and the dry seasons corresponded to a period of decreasing
411 river discharge and groundwater water table level (Figs. 2, 4-5). In each stream order, low-water period and lowest discharges
412 were observed during the long dry season (Fig. 2). The stream orders 1 and 3 were dried up during the long dry season (from
413 the 01st Jan. to the 15th Mar. 2016 and to the 28th Apr. 2016, for stream order 1 and 3, respectively) whereas the streams with
414 orders higher than 3 were never dried up (Fig. 2).

415 **3.2. Seasonal variations of C and ancillary parameters in non-flooded forest groundwater**

416 Yearly averages and ranges in C and ancillary parameters in non-flooded forest groundwater are detailed in Tables 2 and 3.
417 The coefficients of variation of groundwater temperature, pH and specific conductivity were lower than 5% showing a strong
418 stability for these parameters throughout the water cycle. Oxygen saturation in non-flooded forest groundwater increased
419 during the long dry season and peaked at the end of the same season (up to 68% the 30th Mar. 2016), then slowly decreased

420 towards the end of the long rainy season (down to 38% the 15th Nov. 2016) (Fig. 4). pCO₂ in non-flooded forest groundwater
421 concentration exhibited strong temporal variations (coefficient of variation was about 50%), and peaked in the middle of the
422 short (up to 100 000 ppmv the 16th Feb. 2016) and long (up to 200 000 ppmv the 01st Aug. 2016) dry seasons, while decreasing
423 during the two wet seasons (Fig. 4). All year long, DOC in non-flooded forest groundwater was below the detection limit of 1
424 mg L⁻¹ (<83 µmol L⁻¹); note we considered this threshold as the average DOC concentration in non-flooded forest groundwater.
425 Despite one peak of TA that was up to 138 µmol L⁻¹ the 29th Sep. 2016, TA in non-flooded forest groundwater was relatively
426 stable through the water cycle (Fig. 4).

427 **3.3. Seasonal variations of C and ancillary parameters in surface waters**

428 Yearly averages and ranges in C and ancillary parameters in surface waters are detailed in Tables 2 and 3. In streams orders 1
429 and 3 variations of specific conductivity and oxygen saturation were weakly affected by the discharge as indicated by non-
430 correlations between these parameters and the discharge in these streams (Table 4, Fig. 5). Nonetheless, in the stream order 3,
431 we observed an increased in oxygen saturation during dry periods (Fig. 5). On the contrary, in streams orders 4, 5 and 6,
432 variations of pH, specific conductivity and oxygen saturation as a function of river discharge were more pronounced as these
433 parameters peaked during dry seasons and decreased during rainy seasons as indicated by significant negative correlations
434 between these parameters and the discharge in these streams (Table 4, Fig. 5).

435
436 DOC concentration in stream order 1 increased at the beginning of the re-flowing period (i.e., at the beginning of the short
437 rainy season, up to 4 140 µmol L⁻¹ the 14th Apr. 2016) (Fig. 5). In larger streams (order > 1), a similar DOC trend occurred but
438 with a slight delay of about a couple of weeks in comparison to the one observed in stream order 1 (Fig. 5). In all stream orders,
439 after the seasonal peak of DOC at the beginning of the short rainy season, DOC concentration quickly decreased to reach
440 minimum values during the following short dry season, then DOC concentration was rather stable until the next short rainy
441 season (Fig. 5). In stream order 1, POC and TSM concentrations also peaked significantly at the beginning of the re-flowing
442 period, driving the negative correlation of these two parameters with the discharge in stream order 1; we did not observe a
443 similar increase in higher order streams (Table 4; Fig. 5). In addition, in stream order 1, POC%, POC and TSM concentrations
444 increased during the two wet seasons, while decreased during the short dry season; a similar trend was observed in stream
445 orders 5 and 6 as indicated by positive correlations between POC and TSM and the discharge in stream orders 5 and 6 (Table
446 4; Fig. 5). In contrast, in stream orders 3 and 4, TSM concentration did not follow this trend as it peaked during the short dry
447 season and at the beginning of the long dry season (Fig. 5).

448
449 In all stream orders, we observed an increase in TA concentration during the long rainy season followed by a quick decrease
450 (Fig. 5). Overall, there was also a peak in TA concentration at the end of the long dry season followed by a decrease during
451 the following short rainy and dry seasons, driving the significant negative correlations between discharge and TA concentration
452 in stream orders 4, 5 and 6 (Table 4, Fig. 5). In the stream order 1, pCO₂ exhibited a similar trend to the POC, with values

453 peaking during the two wet seasons (Fig. 5). In larger streams (order >1), pCO₂ also seasonally peaked during the long rainy
454 season, but more significantly in stream orders 5 and 6 as indicated by the positive correlations between pCO₂ and discharge
455 in stream orders 5 and 6 (Table 4).

456 **3.4. Spatial variations of C and ancillary parameters across non-flooded forest groundwater, and increasing stream** 457 **orders**

458 TSM and POC concentrations were not significantly different in streams orders 3, 5 and 6, but were significantly lower in
459 stream order 1, while being significantly higher in stream order 4 ($p<0.001$, Kruskal-Wallis with Dunn's multiple comparisons
460 tests) (Fig. 6). POC content of the TSM was significantly higher in stream order 1 in comparison to all other stream orders,
461 while not being significantly different between stream orders 3 to 6 ($p<0.05$, Kruskal-Wallis with Dunn's multiple
462 comparisons tests) (Fig. 6). DOC concentration was not significantly different between streams orders 1, 4, 5 and 6, but was
463 significantly lower in non-flooded forest groundwater, while being significantly higher in stream order 3 ($p<0.001$, Kruskal-
464 Wallis with Dunn's multiple comparisons tests) (Fig. 6).

465

466 The oxygen saturation was not significantly different between non-flooded forest groundwater and streams orders 1, 3 and 4,
467 whereas it was significantly lower in the Nyong River (streams orders 5 and 6) ($p<0.05$, Kruskal-Wallis with Dunn's multiple
468 comparisons tests) (Fig. 6). TA concentration was significantly higher in stream order 1 than in non-flooded forest groundwater
469 ($p>0.01$, Mann-whitney test) (Fig. 6) (Fig. 5). In addition, TA concentration was significantly higher in streams orders 5 and
470 6 than in non-flooded forest groundwater and in streams orders 1, 3 and 4 ($p<0.001$, Kruskal-Wallis with Dunn's multiple
471 comparisons tests) (Fig. 6). pCO₂ was significantly higher in non-flooded forest groundwater, while was similar in all other
472 stream orders ($p<0.001$, Kruskal-Wallis with Dunn's multiple comparisons tests) (Fig. 6), even though pCO₂ decreased overall
473 from stream order 1 to 6 (Table 3).

474 **3.5. C budget at the Mengong catchment scale**

475 The DIC_{budget} was well-balanced, showing inputs and outputs fluxes not statistically different ($p>0.05$; Mann-Whitney test)
476 and differing only by 6% (Table 5), indicating that all DIC fluxes have been considered and well constrained. In contrast, the
477 DOC_{budget} was not balanced, showing statistically different inputs and outputs fluxes ($p<0.001$; Mann-Whitney test) by
478 240%(Table 5), showing that unidentified DOC inputs were overlooked from the estimated budget .The quantity of
479 hydrologically exported C from non-flooded forest groundwater ($F_{GW} + F_{GW-bis}$) was 6.8 ± 3.0 MgC yr⁻¹ (14.1 ± 6.2 MgC km⁻²
480 yr⁻¹), DIC contributing for 97% (Fig. 7). Noteworthy, 10% of the C hydrologically exported from non-flooded forest
481 groundwater goes to the wetland (F_{GW-bis}) rather than the stream (F_{GW}) (Fig. 7). The quantity of hydrologically exported C
482 from wetland to the stream (F_{WL}) was 4.0 ± 1.5 MgC yr⁻¹ (33.0 ± 12.4 MgC km⁻² yr⁻¹); DOC, DIC and POC contributing for 45,
483 45 and 5%, respectively (Fig. 7). The C degassed to the atmosphere as CO₂ (F_D) was 5.5 ± 2.3 MgC-CO₂ yr⁻¹, while the
484 heterotrophic respiration in the stream (F_{RH}) was 0.3 ± 0.3 MgC-CO₂ yr⁻¹ (Fig. 7).

3.6. CO₂ degassing and C export to the ocean at the Nyong watershed scale

Spatially, yearly averages of monthly k_{600} increased from stream order 1 ($2.2 \pm 0.1 \text{ m d}^{-1}$) to 4 (3.0 ± 0.3) and subsequently decreased downstream in stream orders 5 (2.3 ± 0.1) and 6 (2.5 ± 0.2) (Table 6). In contrast, monthly k_{600} did not exhibit much seasonal variations (Table 6; Fig. S2). Spatially, yearly averages of monthly CO₂ degassing rates were similar in stream orders 1, 2, 3 and 4 but significantly lower in stream orders 5 and 6 ($p < 0.001$, Kruskal-Wallis with Dunn's multiple comparisons tests) (Table 6). Rates of heterotrophic respiration were 286 ± 228 and $756 \pm 333 \text{ gC-CO}_2 \text{ m}^{-2} \text{ yr}^{-1}$ in stream order 1 and 5, respectively, whereas CO₂ degassing rates were 5344 ± 2773 and $3706 \pm 1540 \text{ gC-CO}_2 \text{ m}^{-2} \text{ yr}^{-1}$ in the same stream orders, respectively (Table 6). Seasonally, considering all stream orders, the monthly average CO₂ degassing rate during rainy seasons was in average 20% higher in comparison to the average CO₂ degassing rate during dry seasons, explaining higher integrated CO₂ degassing during rainy seasons at the Nyong watershed scale (Fig. 8). In addition, at the Nyong watershed scale, the yearly integrated CO₂ degassing (F_{degas}) was $652 \pm 161 \text{ GgC-CO}_2 \text{ yr}^{-1}$ ($23.4 \pm 5.8 \text{ MgC-CO}_2 \text{ km}^{-2} \text{ yr}^{-1}$ when weighed by the Nyong watershed surface area); and the yearly integrated hydrological C export to the ocean (F_{ocean}) was $12 \pm 10 \text{ GgC yr}^{-1}$ ($0.6 \pm 0.5 \text{ MgC km}^{-2} \text{ yr}^{-1}$) for POC, $134 \pm 100 \text{ GgC yr}^{-1}$ ($7.2 \pm 5.4 \text{ MgC km}^{-2} \text{ yr}^{-1}$) for DOC, and $46 \pm 42 \text{ GgC yr}^{-1}$ ($2.5 \pm 2.3 \text{ MgC km}^{-2} \text{ yr}^{-1}$) for DIC; more than 50% of F_{ocean} occurred during the long rainy season (Tables 6-7; Fig. 8).

4. Discussion

4.1. Non-flooded forest groundwater and wetland as C sources in a first-order catchment

The drainage of non-flooded forest groundwater (i.e., groundwater from the hillside lateritic system) and wetland (i.e., hydromorphic system) fuels the Mengong stream with organic and inorganic C (Figs. 3, 7; Boeglin et al., 2005; Viers et al., 1997). In the hillside lateritic system, overland flow is negligible owing to limited soil erosion due to dense vegetation cover and high soil porosity facilitating rainfall infiltration (Braun et al., 2005; Maréchal et al., 2011). Consequently, hydrological export of soil C to the stream by overland flow from the hillside is considered as negligible. In contrast to the hillside lateritic system, overland flow is a possible C pathway from the hydromorphic wetland system to the stream (Fig. 3; Maréchal et al., 2011). Thus, the stream POC shall originates mostly from the overland flow over the wetland, as also suggested by similar $\delta^{13}\text{C}$ values of total organic carbon (TOC) in the wetland soil and in the POC observed in the stream outlet (range was -28 to -31‰) of the Mengong catchment by Nkoue-Ndondo et al. (2020). The fact that POC and TSM concentrations in the Mengong stream increased during rainy seasons, when the hydrological connectivity with the surrounding wetland is enhanced, is also in a good agreement with the identification of wetland as the main (if not exclusive) source of POC and TSM. Furthermore, Nkoue-Ndondo et al. (2020) did not observe seasonal variations of the $\delta^{13}\text{C}$ -POC signature in the Mengong stream. This suggests that the additional POC source observed at the beginning of the reflowing period also originates from the erosion of the wetland even though this hydrological period was characterized by a weaker hydrological connectivity with the wetland compared to rainy seasons. In the Mengong wetland, litter-fall measurement by Nkoue-Ndondo (2008) was 116 t yr^{-1} of wet

516 OM with a mean C content of 22.5%, which is equivalent to 26 MgC yr⁻¹, a flux 75-times higher than our conservative
517 estimation of the POC leached from the wetland to the stream (0.3 tMgC yr⁻¹, Fig. 7). This implies that most of the wetland
518 litter-fall accumulates in the wetland soil rather than being hydrologically exported to the stream in the form of POC, in
519 particular due to limited overland flow in the wetland due to flat topography (Maréchal et al., 2011). However, the *in-situ*
520 degradation of highly labile OM from litter-fall might contribute to the DOC and DIC fluxes from the wetland to the stream.
521 Indeed, tropical wetlands are recognized as productivity hotspots and a large fraction of the litter-fall is degraded *in-situ* by
522 heterotrophic respiration in the water and sediment, enriching wetland waters in DOC and DIC (Abril et al., 2014; Borges et
523 al., 2015a).

524

525 In the Mengong catchment, waters originating from the drainage of non-flooded forest groundwater and wetland are considered
526 as clear and coloured waters, respectively, the colour reflecting their DOC content (Boeglin et al., 2005; Viers et al., 1997).
527 Indeed, DOC concentration was low in clear waters (<83 µmol L⁻¹) whereas DOC concentration was high in coloured waters
528 (1 420±750 µmol L⁻¹) (Table 3; Viers et al., 1997). The DOC in the soil solution has distinct sources that are litter leaching,
529 root and microbial exudates, rainfall (throughfall and stemflow), and decaying fine roots (Bolan et al., 2011; Kalbitz et al.,
530 2000). Once in the soil solution, DOC is however rapidly adsorbed onto soil minerals during its percolation through the soil
531 column due to the soil capacity for DOC stabilization (Kothawala et al., 2009; Neff and Asner, 2001) by sorption on Fe (and
532 Al) oxides and hydroxides and clay minerals (Kaiser et al., 1996; Kothawala et al., 2009; Sauer et al., 2007). DOC sorption in
533 soils significantly reduces DOC mineralisation rates in soils (Hagedorn et al., 2015; Kalbitz et al., 2005; Kalbitz and Kaiser,
534 2008) and DOC export from soils (Shen et al., 2015). DOC sorption in soils also partly explains the decreasing gradient of
535 DOC concentration with depth commonly observed in boreal (e.g., Moore, 2003), temperate (e.g., Deirmendjian et al., 2018)
536 and tropical (e.g., Johnson et al., 2006) soils. DOC sorption in soils is actually strongly related to the availability of Fe (and
537 Al) oxides and hydroxides, and clay minerals, which are present both in the hillside lateritic and in the hydromorphic wetland
538 soils of the Mengong catchment (Fig. S1). In the hillside lateritic system, soil DOC is probably well stabilized in the iron-rich
539 and clay horizons preventing DOC leaching to the non-flooded forest groundwater (Braun et al., 2005, 2012). Furthermore,
540 DOC must be desorbed from soil minerals in order to be exported to groundwater (Sanderman and Amundson, 2008). Studies
541 have shown that water saturation of the topsoil generates reducing conditions in the saturated soil (Camino-Serrano et al.,
542 2014; Fang et al., 2016) which limits the retention of soil DOC and thus enhances its export to groundwater (Deirmendjian et
543 al., 2018). In the hillside lateritic system, the non-flooded forest groundwater table never reaches the topsoil where soil DOC
544 is high. Therefore, DOC adsorption in these soils might be enhanced. In the hydromorphic wetland system, the groundwater
545 saturates the topsoil all year long (Fig. S1) which might reduce DOC adsorption in this compartment. In addition, hydromorphic
546 conditions occurring in the Mengong wetland soil favour the solubilisation of Fe (Oliva et al., 1999), which is supposed to
547 reduce DOC sorption. Altogether, this explains the low and high DOC concentrations observed in the non-flooded groundwater
548 and the wetland, respectively. In addition, the results showed that stream DOC increased during the first wet season only. In
549 the Mengong catchment, Nkounde-Ndondo (2008) described the piston flow that occurs at the beginning of the short rainy

550 season, which is caused by new infiltration of water on the hills and hillsides that pushes the older soil water downstream (e.g.,
551 Huang et al. (2019) and references therein), allowing pressure on the aquifer and thus exfiltration at the bottom of the slope
552 (i.e., in the wetland; Fig. 3). Consequently, wetland DOC is quickly flushed during the first rains and originates from the
553 subsurface horizons of the wetland soil. Later in the season, the decrease of stream DOC is due to dilution with non-flooded
554 forest groundwater with low DOC content. Noteworthy, our stream DOC budget was not balanced (Table 5; Fig. 7), indicating
555 that sources contributing to the DOC content of the Mengong stream were overlooked. An additional DOC source that was
556 quantified by Braun et al. (2005) during 4 years in the Mengong catchment is DOC in the throughfall. These authors determined
557 that the average DOC concentration in the throughfall was $3.6 \pm 3.5 \text{ mg L}^{-1}$. Applying average DOC concentration in the
558 throughfall to the rainfall in 2016 and the catchment surface area gives an additional DOC input from precipitation of 4.3 ± 4.3
559 MgC yr^{-1} , which allows closing the DOC budget at the Mengong catchment scale.

560

561 Non-flooded forest groundwater and wetland exhibited high DIC concentrations, $2\,940 \pm 1485$ and $1\,430 \pm 900 \text{ } \mu\text{mol L}^{-1}$,
562 respectively and, in both systems, DIC was mostly in the CO_2 form ($>90\%$) (Table 3). Microbial activity has been shown to
563 be limited in many aquifers by the availability of DOC (e.g., Malard and Hervant (1999) and references therein). Thus, non-
564 flooded forest groundwater was free of DOC, CO_2 in non-flooded forest groundwater likely comes from soil respiration in the
565 overlying non-saturated soil - rather than respiration within the groundwater - and then is transported downward by diffusion
566 rather than percolation with rain water. Indeed, the thickness of the lateritic cover on hills and slopes of the Mengong catchment
567 considerably slows the water percolation in the bedrock (Boeglin et al., 2005). In the tropics, the soil respiration rate is mostly
568 affected by soil moisture as soil temperature exhibits low seasonal variations (Davidson et al., 2000). Accordingly, soil
569 respiration rates usually decrease from rainy to dry seasons in tropical ecosystems due to decreasing soil moisture (Davidson
570 et al., 2000; Schewendenmann and Veldkamp, 2006). Nevertheless, in the Mengong catchment, pCO_2 in non-flooded forest
571 groundwater peaked during dry seasons and started to decrease later in the same season and then during the following rainy
572 season (Fig. 4). In mature forest of Amazonia, Johnson et al. (2008) observed a similar trend in groundwater that they attributed
573 to an increase in vegetation water uptake and roots activity in deep soils during the onset of the dry seasons. Indeed, during
574 dry seasons, tropical mature forest depends on deep root system to extract water from the soil and deep root system also provide
575 inorganic and organic C to the deep soil through root respiration and exudation (Nepstad et al., 1994). Furthermore, during dry
576 seasons, the diffusion of CO_2 in the porous soil is facilitated in tropical forest (Adachi et al., 2006) because low soil water
577 content increases air-filled pore space (Schewendenmann and Veldkamp, 2006), very likely favouring the downward diffusion
578 of soil CO_2 and its subsequent dissolution in groundwater, as also observed in temperate forests (Deirmendjian et al., 2018;
579 Tsy-pin and Macpherson, 2012). In the non-flooded forest groundwater, oxygen saturation was about 40% but increased during
580 dry seasons whereas decreasing during rainy seasons (Fig. 4). Atmospheric air can thus penetrate the soil atmosphere deeply,
581 in particular during dry seasons when the diffusion in the porous soil is facilitated, and can reach the non-flooded forest
582 groundwater. In the wetland hydromorphic system, the soil is permanently saturated which limits aerobic respiration of
583 microbes in the soil and leading to the accumulation of OM in the soil profile, likely explaining the lower CO_2 concentration

584 observed in the wetland compared to non-flooded forest groundwater (Table 3). Nonetheless, it should be noted that wetland
585 vegetation can actively transport oxygen to the root zone via their aerenchyma (Haase and Rättsch, 2010), creating a complex
586 oxic-anoxic interface that promotes aerobic respiration but also supplies labile OM to anaerobic degradation (and
587 methanogenesis) fuelling CO₂ (and CH₄) production (Piedade et al., 2010). This is in a good agreement with δ¹³C-DIC
588 signatures of -16‰ measured by Nkoue Ndondo et al. (2020) in the wetland soil, which are indeed close to the C₄ signature
589 of aquatic grassland found in the Mengong wetland. In addition to drainages of non-flooded forest groundwater and wetland,
590 stream DIC can also originate from *in-situ* respiration of DOC. *In-situ* respiration of DOC is corroborated by our results of
591 incubations (Table 6), and by the δ¹³C-DIC at the Mengong stream outlet that was more depleted in ¹³C than in non-flooded
592 forest groundwater and wetland (Nkoue Ndondo et al., 2020), which highlights in-stream respiration from an organic ¹³C-
593 depleted source.

594

595 Non-flooded forest groundwater and wetland both exhibited low TA concentrations, 53±26 and 122±46 μmol L⁻¹, respectively;
596 nonetheless TA concentration was significantly higher in wetland (Table 3; Fig. 6). Considering the granitic lithology (i.e.,
597 absence of carbonate minerals) of the Nyong watershed, TA in non-flooded forest groundwater and wetland might originate
598 from the weathering of silicate minerals as dissolved CO₂ can react with silicate minerals to produce bicarbonates (Meybeck,
599 1987). Applying TA concentration in non-flooded forest groundwater into Equations 11 and 12 results in a silicate weathering
600 rate in the overlying lateritic soil of 0.2±0.1 MgC km⁻² yr⁻¹, whereas applying TA concentration in wetland into Equation 13
601 results in a silicate weathering rate in wetland of 1.3±0.4 MgC km⁻² yr⁻¹. The silicate weathering rate in the wetland soil is thus
602 550% higher than in the non-flooded lateritic soil. Even though these two rates remain low compared to weathering rates in
603 carbonated environment, they are typical of silicate weathering rates which are in the range 0.1-5.2 MgC km⁻² yr⁻¹ as estimated
604 from diverse worldwide basins by Amiotte Suchet et al. (2003). In non-flooded forest groundwater, the low TA concentrations
605 and silicate weathering rates, along with, the absence of significant seasonal variations of TA, are likely related to the relatively
606 inert mineralogy of the lateritic soil cover (Braun et al., 2005, 2012). In the Nyong watershed, the low silicate weathering rates
607 are in a good agreement with the low mineral dissolved load in the aquifer (Braun et al., 2002) and by the dissolved silica
608 fluxes in rivers that were significantly lower compared to the annual rainfall (White and Blum, 1995). In addition, silicate
609 weathering rates in the wetland might be enhanced by the leaching of humic acids from the vegetation to the hydromorphic
610 soils (Braun et al., 2005; Nkoue-ndondo, 2008).

611 **4.2. Influence of wetland-river connectivity on riverine C cycling at the Nyong watershed scale**

612 The role of wetland on riverine C cycling in tropical watersheds is commonly explored using empirical relationships between
613 wetland extent and C concentrations in the stream water of the different sub-catchments of a given watershed. Establishing
614 such empirical relationships in the Nyong watershed is extremely challenging owing the similar wetland extent (about 5% of
615 the surface area; Table 1) in the sub-catchments, with the exception of the first-order Mengong catchment where the wetland
616 extent represents 20%. However, this role can be explored by comparing the seasonality of C concentrations in stream order 1

617 - in which the wetland dynamic as a riverine C source has been discussed in the above section - with respect to the larger
618 streams (order > 1). Thus, for a given parameter, similar seasonality in stream order 1 and the larger streams might suggest
619 that C sources and processes are similar in both (sub)systems.

620

621 Similarly to what we observed in the Mengong catchment, wetlands might be also considered as the main source of POC for
622 surface waters in the whole Nyong watershed based on (1) the low slopes in the watershed, (2) the high infiltration capacity of
623 the soil, (3) the similar normalized export of POC from wetland to the Mengong stream (order 1) and from the Nyong watershed
624 to the ocean (Tables 5 and 7), and (4) the probable low pelagic primary production in the surface waters of the Nyong
625 watershed, as usually observed in tropical rivers with high DOC concentrations ($>1\ 500\ \mu\text{mol L}^{-1}$) where light attenuation
626 caused by browning (coloured waters) strongly limits aquatic photosynthesis (Borges et al. 2019). Moreover, the seasonality
627 of POC was similar in stream order 1 and in high-order streams, increasing during rainy seasons while decreasing during dry
628 seasons (Fig. 5). Thus, the POC leached from wetlands from low-order catchments might acts as an important POC source to
629 high-order streams. However, during rainy seasons, the higher POC concentration observed in high-order streams in
630 comparison to the stream order 1 (Figs. 5-6) might also suggests an additional POC source in in high-order streams during
631 rainy seasons. In high-order streams, given that POC% increased during rainy seasons, river bed and banks erosion is not likely
632 as this process would have exported more TSM than POC, as observed in the tropical Tana River in Kenya by Tamooch et al.
633 (2012). As pelagic primary production is also unlikely, POC leached from wetlands riparian to high-order streams and POC
634 leached from floating macrophytes that develops in the river bed of high-order streams during the dry seasons anterior to the
635 rainy seasons are more suitable hypotheses to explain the additional POC source observed in high-order streams during rainy
636 seasons. Indeed, as in the Amazonian basin (e.g., Abril et al., 2014; Engle et al., 2008; Silva et al., 2013), we observed in high-
637 order streams the development of floating macrophytes during dry seasons. In high-order streams, the development of these
638 floating macrophytes was accompanied by peaks of oxygen saturation during dry seasons (Table 4; Fig. 5). This last feature is
639 in line with the high photosynthesis capacity of macrophytes that results in oxygen-enriched water during daylight (Sabater et
640 al., 2000). According to the flood pulse concept in tropical rivers by Junk et al. (1989), floating macrophytes might be
641 hydrologically exported during rainy seasons when the river discharge increased sufficiently. In high-order streams of the
642 Nyong watershed, the seasonal wetland and floating macrophytes flush of C and OM is also supported by other evidences such
643 as higher pCO_2 and POC% along with lower oxygen saturation observed in these streams. On the one hand, these features
644 might be attributed to enhanced heterotrophic respiration in the river fuelled by export of freshly-produced and young OM
645 (Engle et al., 2008; Mayorga et al., 2005; Tamooch et al., 2014). Moreover, OM leached from tropical wetland can be
646 photodegraded downstream into more labile lower molecular weight compounds that in turn also enhances heterotrophic
647 respiration in the river, as observed in the Congo River by Lambert et al. (2016). On the other hand, the drainage of wetland
648 can also directly account for CO_2 emissions from surface waters as under flooded conditions, roots and microbial respiration
649 occurring in wetland directly release CO_2 to the water (Abril et al., 2014; Moreira-Turcq et al., 2013). These two patterns
650 usually explain the positive correlation between pCO_2 and river discharge in tropical systems (Table 4; Borges et al., 2019).

On the contrary, during dry periods, the wetlands are shrinking and the river become more hydrologically disconnected from wetlands, explaining the lower $p\text{CO}_2$ in tropical rivers during dry seasons (Abril and Borges, 2019). The importance of river-wetland connectivity was also evidenced by the first POC increase at the beginning of the re-flowing period that was not observed downstream (Fig. 5). This suggests POC was quickly oxidized *in-situ*, or did not reach downstream due to weak hydrological connectivity with high-order streams during this period. Indeed, when the Mengong stream (order 1) was flowing again, the downstream Awout River (order 3) was still dry. This highlights the complex deposition and remobilisation cycles of TSM and POC in tropical rivers (Geeraert et al., 2017; Moreira-Turcq et al., 2013). Finally, in stream orders 3 and 4, we observed an additional increase of TSM during dry seasons, while POC% decreased (Fig. 5). This suggests that more TSM than POC was leached into these streams during dry seasons. We assume that river bed and banks erosion could drive this seasonal trend. In the tropical Tana River in Kenya, based on radionuclide's ratio reflecting the age of TSM, Tamooch et al. (2014) showed that TSM was old and increased during dry seasons. This was attributed to inputs of older sediments, with river banks erosion and/or resuspended sediments suggested as the main sources.

663

In surface waters, in contrast to $p\text{CO}_2$ and POC data, we did not observe a positive correlation between DOC and the river discharge, in agreement with Brunet et al. (2009) who showed that DOC in the Nyong watershed was only flushed during a short period of time at the beginning of the short rainy season (Fig. 5). In contrast to POC, DOC did not peak a second time during the long rainy season (Fig. 5). We have no explanation to this, except the fact that this probable second flush of DOC was faster than our fortnightly sampling frequency. Nonetheless, DOC exhibited a similar seasonality in stream order 1 and high-order streams, but with a slight lag time due to the time the water needs to flow from upstream to downstream showing that wetland from low-order streams are significant sources of DOC for downstream rivers. In addition, in the Awout River (order 3), a significant increase in DOC was observed at the beginning of the reflowing period indicating an additional source of DOC (Fig. 5). Actually, before the reflowing period, the bed of the Awout River (order 3) was completely vegetated by large macrophytes (up to 2 m tall) and many small pockets of stagnating water remained. DOC could accumulate in these stagnating waters and be remobilized when the water flows again, as observed in temperate rivers (Deirmendjian et al., 2019; Sanders et al., 2007). The seasonal wetland flush in high-order streams can be also evidenced by peaks of TA during the long rainy seasons, while the increase in TA in streams orders 5 and 6 during the long dry season could not be explained by wetland inputs to river. In stream orders 5 and 6, during the long dry season, surface waters are likely fed by deeper groundwater, which are older and likely characterized by higher TA concentrations than shallower levels, as observed in temperate (Deirmendjian and Abril, 2018) and tropical (Duvert et al., 2020b) catchments. Duvert et al. (2020b) gave additional evidence of a shift from biogenic (wetlands) to geogenic C source during dry seasons caused by changing water sources.

4.3. C fluxes at the plot (first-order) and the watershed scales

At the first-order Mengong catchment scale, each fluxes of the stream C budget were estimated independently. Hydrological C inputs from wetland (F_{WL}) and non-flooded forest groundwater (F_{GW}) to the stream contributed to 38% ($4.0 \pm 1.5 \text{ MgC yr}^{-1}$)

684 and 62% ($6.2 \pm 3.0 \text{ MgC yr}^{-1}$) of the total hydrological C inputs, respectively (Table 5; Fig. 7). However, when the later fluxes
 685 are weighed by respective surface area, F_{WL} and F_{GW} contributed to 73% ($33.0 \pm 12.4 \text{ MgC yr}^{-1}$) and 27% ($13.0 \pm 6.2 \text{ MgC yr}^{-1}$)
 686 of the total hydrological C inputs to the stream, respectively (Fig. 7). In the first-order Mengong catchment, 83% and 17% of
 687 the CO_2 degassing (58% and 42% if weighed by surface area) from the stream are sustained by inputs of DIC from non-flooded
 688 forest groundwater and wetland, respectively (Fig. 7). At the Nyong watershed scale; our study design did not allow to estimate
 689 the contributions of CO_2 degassing from non-flooded forest groundwater and wetland. However, we might assume that the
 690 wetland contribution to CO_2 degassing become greater with increasing stream order, particularly considering larger riparian
 691 wetlands in high-order streams and the development of floating macrophytes in river bed during dry seasons (Olivry, 1986).
 692 Nonetheless, our results are in line with the growing consensus that tropical wetlands contribute significantly to the C inputs
 693 in tropical rivers (Abril et al., 2014; Borges et al., 2015a, 2019, 2015b; Duvert et al., 2020a, 2020b). In the Mengong catchment,
 694 an important fraction (~50%) of the C entering the stream directly returns to the atmosphere through CO_2 degassing at the
 695 water-air interface (Fig. 7); the remaining C is transported, processed and further degassed downstream (Abril et al., 2014). In
 696 the Nyong watershed, our estimated k_{600} are typical of lowland tropical rivers (e.g., Alin et al., 2011; Borges et al., 2019). The
 697 weak seasonality of our k_{600} shows that higher CO_2 degassing rates during rainy seasons are rather a function of the increase
 698 of CO_2 water-air gradient during rainy seasons - which is due to seasonal flush of wetland and macrophytes - rather than the
 699 increase in k_{600} usually observed during high water periods because of increasing water turbulence. In the Nyong watershed,
 700 the average heterotrophic respiration in the river (pelagic plus benthic) rate was $521 \pm 403 \text{ gC-CO}_2 \text{ m}^{-2} \text{ yr}^{-1}$ whereas the average
 701 CO_2 degassing rate was $5085 \pm 2544 \text{ gC-CO}_2 \text{ m}^{-2} \text{ yr}^{-1}$ (Table 6). Consequently, only ~10% of the degassing at the water-air
 702 interface was supported by heterotrophic respiration in the river. These rates are consistent with measurements by Borges et
 703 al. (2019), who showed that, in the Congo basin, the heterotrophic respiration (pelagic only) in the river averaged 355 gC-CO_2
 704 $\text{m}^{-2} \text{ yr}^{-1}$ and represented ~11% of the average CO_2 degassing rate of $3240 \text{ gC-CO}_2 \text{ m}^{-2} \text{ yr}^{-1}$. In the same way, heterotrophic
 705 respiration in the river accounts for less than 20% of the CO_2 degassing flux from the Amazon Basin (Abril et al., 2014).
 706 Moreover, in the Nyong watershed, the ratio between rates of CO_2 degassing and heterotrophic respiration in the river
 707 decreased in the stream order 5 (ratio of 4.9) compared to stream order 1 (ratio of 18.6) (Table 6). This is in line with the recent
 708 findings by Hotchkiss et al. (2015) in temperate rivers, where they showed that the contribution of internal metabolism to
 709 account for CO_2 emissions increased from upstream to downstream, or with the more recent findings by Borges et al. (2019)
 710 in the Congo basin who found a ratio of CO_2 degassing to heterotrophic respiration in the river rates of 29-137 and 3-17 in
 711 low-and high-order streams, respectively. Borges et al. (2019) attributed their observations to the prevalence of lateral CO_2
 712 inputs in sustaining CO_2 emissions.

713

714 In the Nyong watershed, about 6% ($0.6 \pm 0.5 \text{ MgC km}^{-2} \text{ yr}^{-1}$), 69% ($7.2 \pm 5.4 \text{ MgC km}^{-2} \text{ yr}^{-1}$) and 24% ($2.5 \pm 2.3 \text{ MgC km}^{-2} \text{ yr}^{-1}$)
 715 of the F_{ocean} occurs in the POC, DOC and DIC forms, respectively (Table 7). These C exports to the ocean are consistent but
 716 slightly different from those reported by Meybeck (1993) for rivers in tropical humid regions, as he estimated that 20% (1.9

717 $\text{MgC km}^{-2} \text{ yr}^{-1}$), 53% ($5.1 \text{ MgC km}^{-2} \text{ yr}^{-1}$) and 27% ($2.6 \text{ MgC km}^{-2} \text{ yr}^{-1}$) occurs in the POC, DOC and DIC forms, respectively.
 718 Therefore, in the Nyong watershed, the export of DIC to the ocean was typical of humid tropical regions while the export of
 719 POC was lower and DOC was higher. In the Nyong watershed, lower POC export to the ocean might be explained by the low
 720 watershed slope and the negligible overland flow that limits soil erosion. In contrast, DOC concentration in the surface waters
 721 of the Nyong watershed was in the upper range of those reported for other African rivers (range is 50 to $4\,270 \mu\text{mol L}^{-1}$;
 722 Tamooch et al. 2014 and references therein), thereby driving the higher DOC export to the ocean, which might be explained by
 723 higher wetland extent than in the other African rivers. Huang et al. (2012) estimated the quantity of C exported to the ocean
 724 from African tropical rivers (30°N - 30°S) at 0.3, 1 and $0.6 \text{ MgC km}^{-2} \text{ yr}^{-1}$ for the POC, DOC and DIC forms, respectively, but
 725 they did not partition these tropical rivers in humid or dry climates; our estimations of C export to the ocean were significantly
 726 higher for the tropical Nyong watershed in humid climate region. This shows the importance to upscale C fluxes for the same
 727 climatic regions, such as the widely used Koppen-Geiger climate classification system (Koppen, 1936) recently updated by
 728 Peel et al. (2007), otherwise upscaling might be strongly biased. In the Nyong watershed, the ratio between the C exported to
 729 the ocean and the CO_2 emitted to the atmosphere is 1:0.3, in agreement with ratio of 1:0.2 measured by Borges et al. (2015b)
 730 in the Congo River but contrasting with the global ratio of 1:1 estimated by Ciais et al. (2013) during the Fifth Assessment
 731 Report of the Intergovernmental Panel on Climate Change (IPCC), showing that at least African rivers but probably all tropical
 732 rivers are strong emitters of CO_2 . Therefore, biogeochemical data in African rivers are urgently required to improve accuracy
 733 of regional and global CO_2 emission estimates from inland waters, and understand how they will respond to climate change
 734 (warming, change in hydrological cycle).

735

736 The integration of the different C fluxes was done by comparing them with the terrestrial C budget. In the Mengong catchment,
 737 the total hydrological export of C from land and wetland (F_{GW} , $F_{\text{GW-bis}}$, F_{WL}) represents ~3-5% of the catchment net C sink
 738 (range $201\text{-}336 \text{ MgC yr}^{-1}$) (Fig. 7). This low hydrological C export to the aquatic environment relative to the catchment net C
 739 sink agrees with two plot studies in temperate ecosystems, which have shown that the hydrological export of C from forest
 740 ecosystems is ~3% (Deirmendjian et al., 2018; Kindler et al., 2011). In the Nyong watershed, the yearly CO_2 degassed (F_{degas})
 741 from the river network and the C hydrologically exported to the ocean (F_{ocean}) represented together ~10% of the net terrestrial
 742 C sink estimated by Brunet et al. (2009) (Table 7). Similarly, Duvert et al. (2020a) estimated that the C degassed to the
 743 atmosphere and hydrologically exported at the river outlet represented ~7% of the local net terrestrial C sink in the small (140
 744 km^2) tropical Howard catchment in Australia, ~20% if accounting to C losses via fire. In contrast, from a modelling approach
 745 in the entire Amazon watershed, Hastie et al. (2019) found that C degassed and hydrologically exported might represents 78%
 746 of the net terrestrial C sink. This is in line with findings of Abril et al. (2014) and Borges and al. (2019) who respectively found
 747 that CO_2 degassed from the Amazon and Congo watersheds was greater than the local net terrestrial C sink. Besides, Abril et
 748 al. (2014) attributed CO_2 degassing from rivers to wetland C inputs as they showed that tropical wetland may hydrologically
 749 export 36-80% of their gross primary production (GPP) while terrestrial landscapes hydrologically export few percent of their
 750 net C sink, between 3% for forests and 13% from grasslands (Kindler et al., 2011). Altogether, this shows that in large

watersheds such as the Amazon or the Congo rivers, fluvial C losses could offset more significantly the local net terrestrial C sink compared to relatively small tropical watersheds such as the Nyong or the Howard rivers, which is likely due to both more extensive wetland and greater hydrological fluxes in the Amazon and the Congo.

Conclusions

In a first-order catchment, we showed here by determining all the terms of the C mass balance independently that attributing the whole amount of the CO₂ emitted to the atmosphere and C exported to the stream outlet to a unique terrestrial source and ignoring the river–wetland connectivity might lead to the misrepresentation of C dynamics in small tropical catchments and thus likely at larger scales. Indeed, in addition to the drainage of non-flooded forest groundwater to the stream, we highlighted the drainage and erosion of wetland as an important C source for the stream. Non-flooded forest groundwater was a significant source of C for surface waters, particularly for CO₂, whereas in contrast, DOC and POC in surface waters were mainly provided by the drainage and erosion of wetlands. The flush of C from wetland to first-order streams is seasonally enhanced during rainy seasons when the connectivity with surface waters is greater, allowing the leaching of freshly and young OM to the stream, and thus increasing heterotrophic respiration in the river downstream. Nonetheless, at the Nyong watershed scale, the CO₂ emissions from the entire river network remained largely sustained by direct inputs of CO₂ from land and wetland, as heterotrophic respiration in the river represents only ~10% of the CO₂ degassing at the water-air interface. Moreover, at the Nyong watershed scale, we showed that the CO₂ degassed from the entire river network and C hydrologically exported to the ocean might offset ~11% of the net terrestrial C sink estimated from the watershed. This study supports the view that African rivers are strong emitters of CO₂ to the atmosphere, mostly sustained by wetland inputs, and this must be better considered in global models.

Data availability

The dataset of C and ancillary parameters is publicly available at zenodo.org (Moustapha et al., 2021).

Competing interests

The authors declare they have no conflict of interest.

Acknowledgments

The Nyong Watershed is included in the CZO Multiscale TROPical CatchmentS (M-TROPICS, <https://mtropics.obs-mip.fr>), LMI PICASS-EAU (<https://picass-eau.ird.fr>), LMI DYCOFAC (<https://lab.ird.fr/collaboration/37/show>) and OZCAR (Critical Zone Observatories: Research and Application) funded by IRD (Research Institute for Development—Institut de

778 Recherche sur le Développement) and INSU/CNRS. We thank our colleagues from IRGM (Yaoundé, Cameroon) involved in
 779 M-TROPICS for their help in the field and in the laboratory. M. M. was funded by the French Embassy in Cameroon (Mobility
 780 Fellowship) and L. D. by IRD (Post-Doctoral fellowship). This research was supported by IRD and by Strategic planning
 781 “PSIP Seq2C” (Interdisciplinary and Partnership Structuring Program on Continental Carbon Sequestration). We warmly
 782 thank the two anonymous reviewers and S. Winton together with the editors T. Treude and J.-H. Park for they constructive
 783 comments that greatly improved the manuscript.

784 References

- 785 Åberg, J. and Wallin, B.: Evaluating a fast headspace method for measuring DIC and subsequent calculation of pCO₂ in
 786 freshwater systems, *Int. Waters*, 4(2), 157–166, doi:10.5268/IW-4.2.694, 2014.
- 787 Abril, G. and Borges, A. V.: Carbon leaks from flooded land : do we need to re-plumb the inland water Ideas and perspectives :
 788 Carbon leaks from flooded land: do we need to replumb the inland water active pipe ?, *Biogeoscience*, 16, 769–784,
 789 doi:10.5194/bg-16-769-2019, 2019.
- 790 Abril, G., Martinez, J. M., Artigas, L. F., Moreira-Turcq, P., Benedetti, M. F., Vidal, L., Meziane, T., Kim, J. H., Bernardes,
 791 M. C., Savoye, N., Deborde, J., Souza, E. L., Albéric, P., Landim De Souza, M. F. and Roland, F.: Amazon River carbon
 792 dioxide outgassing fuelled by wetlands, *Nature*, 505(7483), 395–398, doi:10.1038/nature12797, 2014.
- 793 Abril, G., Bouillon, S., Darchambeau, F., Teodoru, C. R., Marwick, T. R., Tamooch, F., Ochieng Omengo, F., Geeraert, N.,
 794 Deirmendjian, L., Polsenaere, P. and Borges, A. V.: Technical note: Large overestimation of pCO₂ calculated from
 795 pH and alkalinity in acidic, organic-rich freshwaters, *Biogeosciences*, 12(1), 67–78, doi:10.5194/bg-12-67-2015, 2015.
- 796 Alin, S. R., Rasera, M. D. F. F. L., Salimon, C. I., Richey, J. E., Holtgrieve, G. W., Krusche, A. V. and Snidvongs, A.: Physical
 797 controls on carbon dioxide transfer velocity and flux in low-gradient river systems and implications for regional carbon
 798 budgets, *J. Geophys. Res. Biogeosciences*, 116(1), doi:10.1029/2010JG001398, 2011.
- 799 Allen, G. H. and Pavelsky, T. M.: Global extent of rivers and streams, *Science* (80-.), 361(6402), 585–588,
 800 doi:10.1126/science.aat0636, 2018.
- 801 Amiotte Suchet, P., Probst, J. and Ludwig, W.: Worldwide distribution of continental rock lithology: Implications for the
 802 atmospheric / soil CO₂ uptake by continental weathering and alkalinity river transport to the oceans, *Global Biogeochem.*
 803 *Cycles*, 17(2), doi:10.1029/2002GB001891, 2003.
- 804 Audry, S., Bessa, H. A., Bedimo, J.-P. B., Boeglin, J.-L., Boithias, L., Braun, J.-J., Dupré, B., Fauchaux, M., Lagane, C.,
 805 Maréchal, J.-C., Ndam-Ngoupayou, J. R., Nnomo, B. N., Nlozo, J., Ntonga, J.-C., Ribolzi, O., Riotte, J., Rochelle-Newall, E.
 806 and Ruiz, L.: The Multiscale TROPICAL CatchmentS critical zone observatory M-TROPICS dataset I: The Nyong River Basin,
 807 Cameroon, *Hydrol. Process.*, 35(5), e14138, doi:10.1002/HYP.14138, 2021.
- 808 Boeglin, J.-L., Ndam, J.-R. and Braun, J.-J.: Composition of the different reservoir waters in a tropical humid area: example
 809 of the Nsimi catchment (Southern Cameroon), *J. African Earth Sci.*, 37(1–2), 103–110, 2003.

810 Boeglin, J. ., Probst, J., Ndam-Ngoupayou, J., Nyeck, B., Etcheber, H., Mortatti, J. and Braun, J. .: Soil carbon stock and river
811 carbon fluxes in humid tropical environments: the Nyong river basin (south Cameroon), in *Soil Erosion and Carbon Dynamics*,
812 *Adv. Soil Sci*, pp. 275–288, CRC Press Boca Raton, Fla., 2005.

813 Bolan, N. S., Adriano, D. C., Kunhikrishnan, A., James, T., Mcdowell, R. and Senesi, N.: *Dissolved Organic Matter*, 1st ed.,
814 Elsevier Inc., 2011.

815 Borges, A. V., Abril, G., Darchambeau, F., Teodoru, C. R., Deborde, J., Vidal, L. O., Lambert, T. and Bouillon, S.: Divergent
816 biophysical controls of aquatic CO₂ and CH₄ in the World's two largest rivers, *Sci. Rep.*, 5, 15614,
817 doi:<https://doi.org/10.1038/srep15614>, 2015a.

818 Borges, A. V., Darchambeau, F., Lambert, T. and Morana, C.: Variations of dissolved greenhouse gases (CO₂ , CH₄ , N₂O)
819 in the Congo River network overwhelmingly driven by fluvial-wetland connectivity, *Biogeosciences*, 16(19), 3801–3834,
820 doi:10.5194/bg-2019-68, 2019.

821 Borges, A. V, Darchambeau, F., Teodoru, C. R., Marwick, T. R., Tamooch, F., Geeraert, N., Omengo, F. O., Guérin, F.,
822 Lambert, T., Morana, C., Okuku, E. and Bouillon, S.: Globally significant greenhouse-gas emissions from African inland
823 waters, *Nat. Geosci.*, 8(8), 637–642, doi:10.1038/NGEO2486, 2015b.

824 Braun, J.-J., Dupré, B., Viers, J., Ngoupayou, J. R. N., Bedimo, J.-P. B., Sighe-Nkamdjou, L., Freydier, R., Robain, H., Nyeck,
825 B. and Bodin, J.: Biogeohydrodynamic in the forested humid tropical environment: the case study of the Nsimi small
826 experimental watershed (south Cameroon), *Bull. la Société géologique Fr.*, 173(4), 347–357, 2002.

827 Braun, J.-J., Ngoupayou, J. R. N., Viers, J., Dupre, B., Bedimo, J.-P. B., Boeglin, J.-L., Robain, H., Nyeck, B., Freydier, R.
828 and Nkamdjou, L. S.: Present weathering rates in a humid tropical watershed: Nsimi, South Cameroon, *Geochim. Cosmochim.*
829 *Acta*, 69(2), 357–387, 2005.

830 Braun, J.-J., Marechal, J.-C., Riotte, J., Boeglin, J.-L., Bedimo, J.-P. B., Ngoupayou, J. R. N., Nyeck, B., Robain, H., Sekhar,
831 M. and Audry, S.: Elemental weathering fluxes and saprolite production rate in a Central African lateritic terrain (Nsimi, South
832 Cameroon), *Geochim. Cosmochim. Acta*, 99, 243–270, 2012.

833 Brunet, F., Dubois, K., Veizer, J., Ndong, G. R. N., Ngoupayou, J. R. N., Boeglin, J. L. and Probst, J. L.: Terrestrial and
834 fluvial carbon fluxes in a tropical watershed: Nyong basin, Cameroon, *Chem. Geol.*, 265(3), 563–572,
835 doi:<https://doi.org/10.1016/j.chemgeo.2009.05.020>, 2009.

836 Camino-Serrano, M., Gielen, B., Luyssaert, S., Ciais, P., Vicca, S., Guenet, B., Vos, B. De, Cools, N., Ahrens, B., Altaf Arain,
837 M., Borken, W., Clarke, N., Clarkson, B., Cummins, T., Don, A., Pannatier, E. G., Laudon, H., Moore, T., Nieminen, T. M.,
838 Nilsson, M. B., Peichl, M., Schwendenmann, L., Siemens, J. and Janssens, I.: Linking variability in soil solution dissolved
839 organic carbon to climate, soil type, and vegetation type, *Global Biogeochem. Cycles*, 28(5), 497–509,
840 doi:<https://doi.org/10.1002/2013GB004726>, 2014.

841 Cardoso, S. J., Enrich-Prast, A., Pace, M. L. and Roland, F.: Do models of organic carbon mineralization extrapolate to warmer
842 tropical sediments?, *Limnol. Oceanogr.*, 59(1), 48–54, 2014.

843 Ciais, P., Sabine, C., Bala, G., Bopp, L., Brovkin, V., Canadell, J. G., Chhabra, A., Defries, R., Galloway, J., Heimann, M.,

844 Jones, C., Le Quéré, C., Myeni, R., Piao, S. and Thornton, P.: Carbon and Other Biogeochemical Cycles., 2013.

845 Cole, J. J. and Caraco, N. F.: Carbon in catchments : connecting terrestrial carbon losses with aquatic metabolism, , 101–110,

846 2001.

847 Cole, J. J., Prairie, Y. T., Caraco, N. F., Mcdowell, W. H., Tranvik, L. J., Striegl, R. G., Duarte, C. M., Kortelainen, P.,

848 Downing, J. A., Middelburg, J. J. and Melack, J.: Plumbing the Global Carbon Cycle : Integrating Inland Waters into the

849 Terrestrial Carbon Budget, *Ecosystems*, 10(1), 172–185, doi:10.1007/s10021-006-9013-8, 2007.

850 Davidson, E. A., Verchot, L. V., Cattânio, J. H., Ackerman, I. L. and Carvalho, J. E. M.: Effects of soil water content on soil

851 respiration in forests and cattle pastures of eastern Amazonia, *Biogeochemistry*, 48, 53–69, 2000.

852 Deirmendjian, L. and Abril, G.: Carbon dioxide degassing at the groundwater-stream-atmosphere interface : isotopic

853 equilibration and hydrological mass balance in a sandy watershed, *J. Hydrol.*, 558, 129–143,

854 doi:10.1016/j.jhydrol.2018.01.003, 2018.

855 Deirmendjian, L., Loustau, D., Augusto, L., Lafont, S., Chipeaux, C., Poirier, D. and Abril, G.: Hydro-ecological controls on

856 dissolved carbon dynamics in groundwater and export to streams in a temperate pine forest, *Biogeosciences*, 15(2), 669–691,

857 doi:10.5194/bg-15-669-2018, 2018.

858 Deirmendjian, L., Anschutz, P., Morel, C., Mollier, A., Augusto, L., Loustau, D., Cotovicz, L. C., Buquet, D., Lajaunie, K.,

859 Chaillou, G., Voltz, B., Charbonnier, C., Poirier, D. and Abril, G.: Importance of the vegetation-groundwater-stream

860 continuum to understand transformation of biogenic carbon in aquatic systems – A case study based on a pine-maize

861 comparison in a lowland sandy watershed (Landes de Gascogne, SW France), *Sci. Total Environ.*,

862 doi:10.1016/j.scitotenv.2019.01.152, 2019.

863 Drake, T. W., Raymond, P. A. and Spencer, R. G. M.: Terrestrial carbon inputs to inland waters: A current synthesis of

864 estimates and uncertainty, *Limnol. Oceanogr. Lett.*, 3(3), 132–142, doi:10.1002/lol2.10055, 2018.

865 Duvert, C., Hutley, L. B., Beringer, J., Bird, M. I., Birkel, C., Maher, D. T., Northwood, M., Rudge, M., Setterfield, S. A. and

866 Wynn, J. G.: Net landscape carbon balance of a tropical savanna: Relative importance of fire and aquatic export in offsetting

867 terrestrial production, *Glob. Chang. Biol.*, 26(10), 5899–5913, doi:10.1111/GCB.15287, 2020a.

868 Duvert, C., Hutley, L. B., Birkel, C., Rudge, M., Munksgaard, N. C., Wynn, J. G., Setterfield, S. A., Cendón, D. I. and Bird,

869 M. I.: Seasonal shift from biogenic to geogenic fluvial carbon caused by changing water sources in the wet-dry tropics, *J.*

870 *Geophys. Res. Biogeosciences*, 125(2), e2019JG005384, 2020b.

871 Engle, diana I., Melack, J. m, Doyle, robert D. and fisher, T. r: High rates of net primary production and turnover of floating

872 grasses on the Amazon floodplain: implications for aquatic respiration and regional CO₂ flux, *Glob. Chang. Biol.*, 14(2), 369–

873 381, doi:10.1111/J.1365-2486.2007.01481.X, 2008.

874 Fang, W., Wei, Y., Liu, J., Kosson, D., Management, H. van der S.-W. and 2016, U.: Effects of aerobic and anaerobic biological

875 processes on leaching of heavy metals from soil amended with sewage sludge compost, *Elsevier, Waste mana*(58), 324–334,

876 2016.

877 Friedlingstein, P., O’Sullivan, M., Jones, M. W., Andrew, R. M., Hauck, J., Olsen, A., Peters, G. P., Peters, W., Pongratz, J.,

878 Sitch, S., Le Quéré, C., Canadell, J. G., Ciais, P., Jackson, R. B., Alin, S., Aragão, L. E. O. C., Arneeth, A., Arora, V., Bates,
879 N. R., Becker, M., Benoit-Cattin, A., Bittig, H. C., Bopp, L., Bultan, S., Chandra, N., Chevallier, F., Chini, L. P., Evans, W.,
880 Florentie, L., Forster, P. M., Gasser, T., Gehlen, M., Gilfillan, D., Gkritzalis, T., Gregor, L., Gruber, N., Harris, I., Hartung,
881 K., Haverd, V., Houghton, R. A., Ilyina, T., Jain, A. K., Joetzjer, E., Kadono, K., Kato, E., Kitidis, V., Korsbakken, J. I.,
882 Landschützer, P., Lefèvre, N., Lenton, A., Lienert, S., Liu, Z., Lombardozzi, D., Marland, G., Metzl, N., Munro, D. R., Nabel,
883 J. E. M. S., Nakaoka, S. I., Niwa, Y., O'Brien, K., Ono, T., Palmer, P. I., Pierrot, D., Poulter, B., Resplandy, L., Robertson, E.,
884 Rödenbeck, C., Schwinger, J., Séférian, R., Skjelvan, I., Smith, A. J. P., Sutton, A. J., Tanhua, T., Tans, P. P., Tian, H.,
885 Tilbrook, B., Van Der Werf, G., Vuichard, N., Walker, A. P., Wanninkhof, R., Watson, A. J., Willis, D., Wiltshire, A. J., Yuan,
886 W., Yue, X. and Zaehle, S.: Global Carbon Budget 2020, *Earth Syst. Sci. Data*, 12(4), 3269–3340, doi:10.5194/ESSD-12-
887 3269-2020, 2020.

888 Gaillardet, J., Braud, I., Hankard, F., Anquetin, S., Bour, O., Dorfliger, N., de Dreuz, J. R., Galle, S., Galy, C., Gogo, S.,
889 Gourcy, L., Habets, F., Laggoun, F., Longuevergne, L., Le Borgne, T., Naaim-Bouvet, F., Nord, G., Simonneaux, V., Six, D.,
890 Tallec, T., Valentin, C., Abril, G., Allemand, P., Arènes, A., Arfib, B., Arnaud, L., Arnaud, N., Arnaud, P., Audry, S., Comte,
891 V. B., Batiot, C., Battais, A., Bellot, H., Bernard, E., Bertrand, C., Bessière, H., Binet, S., Bodin, J., Bodin, X., Boithias, L.,
892 Bouchez, J., Boudevillain, B., Moussa, I. B., Branger, F., Braun, J. J., Brunet, P., Caceres, B., Calmels, D., Cappelaere, B.,
893 Celle-Jeanton, H., Chabaux, F., Chalikakis, K., Champollion, C., Copard, Y., Cotel, C., Davy, P., Deline, P., Delrieu, G.,
894 Demarty, J., Dessert, C., Dumont, M., Emblanch, C., Ezzahar, J., Estèves, M., Favier, V., Fauchaux, M., Filizola, N.,
895 Flammarion, P., Floury, P., Fovet, O., Fournier, M., Francez, A. J., Gandois, L., Gascuel, C., Gayer, E., Genthon, C., Gérard,
896 M. F., Gilbert, D., Gouttevin, I., Grippa, M., Gruau, G., Jardani, A., Jeanneau, L., Join, J. L., Jourde, H., Karbou, F., Labat,
897 D., Lagadeuc, Y., Lajeunesse, E., Lastennet, R., Lavado, W., Lawin, E., Lebel, T., Le Bouteiller, C., Legout, C., Lejeune, Y.,
898 Le Meur, E., Le Moigne, N., Lions, J., et al.: OZCAR: The French Network of Critical Zone Observatories, *Vadose Zo. J.*,
899 17(1), 180067, doi:10.2136/VZJ2018.04.0067, 2018.

900 Geeraert, N., Omengo, F. O., Borges, A. V., Govers, G. and Bouillon, S.: Shifts in the carbon dynamics in a tropical lowland
901 river system (Tana River, Kenya) during flooded and non-flooded conditions, *Biogeochemistry*, 132(1–2), 141–163,
902 doi:10.1007/s10533-017-0292-2, 2017.

903 Gómez-Gener, L., Rocher-Ros, G., Battin, T., Cohen, M. J., Dalmagro, H. J., Dinsmore, K. J., Drake, T. W., Duvert, C.,
904 Enrich-Prast, A., Horgby, Å., Johnson, M. S., Kirk, L., Machado-Silva, F., Marzolf, N. S., McDowell, M. J., McDowell, W.
905 H., Miettinen, H., Ojala, A. K., Peter, H., Pumpanen, J., Ran, L., Riveros-Iregui, D. A., Santos, I. R., Six, J., Stanley, E. H.,
906 Wallin, M. B., White, S. A. and Sponseller, R. A.: Global carbon dioxide efflux from rivers enhanced by high nocturnal
907 emissions, *Nat. Geosci.*, 14(5), 289–294, doi:10.1038/S41561-021-00722-3, 2021.

908 Gran, G.: Determination of the equivalence point in potentiometric titrations. Part II, *Analyst*, 77(920), 661–671, 1952.

909 Gumbrecht, T., Román-Cuesta, R. M., Verchot, L. V., Herold, M., Wittmann, F., Householder, E., Herold, N. and Murdiyarso,
910 D.: Tropical and Subtropical Wetlands Distribution version 2, , doi:doi:10.17528/CIFOR/DATA.00058, 2017.

911 Haase, K. and Rätsch, G.: The morphology and anatomy of tree roots and their aeration strategies, in *Amazonian Floodplain*

912 Forests, pp. 141–161, Springer., 2010.

913 Hagedorn, F., Bruderhofer, N., Ferrari, A. and Niklaus, P. A.: Tracking litter-derived dissolved organic matter along a soil
 914 chronosequence using ¹⁴C imaging: Biodegradation, physico-chemical retention or preferential flow?, *Soil Biol. Biochem.*,
 915 88, 333–343, doi:10.1016/J.SOILBIO.2015.06.014, 2015.

916 Hastie, A., Lauerwald, R., Ciais, P. and Regnier, P.: Aquatic carbon fluxes dampen the overall variation of net ecosystem
 917 productivity in the Amazon basin: An analysis of the interannual variability in the boundless, *Wiley Online Libr.*, 25(6), 2094–
 918 2111, doi:10.1111/gcb.14620, 2019.

919 Holgerson, M. A. and Raymond, P. A.: Large contribution to inland water CO₂ and CH₄ emissions from very small ponds, ,
 920 9(February), doi:10.1038/NGEO2654, 2016.

921 Hotchkiss, E. R., Jr, R. O. H., Sponseller, R. A., Butman, D., Klaminder, J., Laudon, H., Rosvall, M. and Information, S.:
 922 Sources of and processes controlling CO₂ emissions change with the size of streams and rivers, *Nat. Geosci.*, 8(9), 696–699,
 923 doi:10.1038/NGEO2507, 2015.

924 Huang, T., Fu, Y., Pan, P. and Chen, C.: Fluvial carbon fluxes in tropical rivers, *Curr. Opin. Environ. Sustain.*, 4(2), 162–169,
 925 2012.

926 Huang, Y., Evaristo, J. and Li, Z.: Multiple tracers reveal different groundwater recharge mechanisms in deep loess deposits,
 927 Elsevier, 353, 204–212, 2019.

928 Johnson, M. S., Lehmann, Æ. J., Couto, E., Filho, J. and Riha, S.: DOC and DIC in flowpaths of Amazonian headwater
 929 catchments with hydrologically contrasting soils, *Biogeochemistry*, 81, 45–57, doi:10.1007/s10533-006-9029-3, 2006.

930 Johnson, M. S., Lehmann, J., Riha, S. J., Krusche, A. V., Richey, J. E., Ometto, J. P. H. B. and Couto, E. G.: CO₂ efflux from
 931 Amazonian headwater streams represents a significant fate for deep soil respiration, *Geophys. Res. Lett.*, 35(17),
 932 doi:10.1029/2008GL034619, 2008.

933 Jones, M. B. and Humphries, S. W.: Impacts of the C₄ sedge *Cyperus papyrus* L. on carbon and water fluxes in an African
 934 wetland, , 107–113, 2002.

935 Junk, W., Bayley, P. and Sparks, R.: The flood pulse concept in river-floodplain system.pdf, *Can. Spec. Publ. Fish. Aquat.*
 936 *Sci.*, 106(1), 110–127, 1989.

937 Kaiser, K., Guggenberger, G. and Zech, W.: Sorption of DOM and DOM fractions to forest soils, *Geoderma*, 74(3–4), 281–
 938 303, doi:10.1016/S0016-7061(96)00071-7, 1996.

939 Kalbitz, K. and Kaiser, K.: Contribution of dissolved organic matter to carbon storage in forest mineral soils, *J. Plant Nutr.*
 940 *Soil Sci.*, 171(1), 52–60, doi:10.1002/JPLN.200700043, 2008.

941 Kalbitz, K., Solinger, S., Park, J., Michalzik, B. and Matzner, E.: Controls on the dynamics of dissolved organic matter in
 942 soils: a review, *Soil Sci.*, 165(4), 277–304, 2000.

943 Kalbitz, K., Schwesig, D., Rethemeyer, J. and Matzner, E.: Stabilization of dissolved organic matter by sorption to the mineral
 944 soil, *Soil Biol. Biochem.*, 37(7), 1319–1331, doi:10.1016/J.SOILBIO.2004.11.028, 2005.

945 Kindler, R., Siemens, J., ... K. K.-G. C. and 2011, undefined: Dissolved carbon leaching from soil is a crucial component of

the net ecosystem carbon balance, Wiley Online Libr., 17(2), 1167–1185, doi:10.1111/j.1365-2486.2010.02282.x, 2011.

Koppen, W.: Das geographische System der Klimate, in Handbuch der Klimatologie, edited by B. Köppen, W. and Geiger, G., 1. C. Gebr, pp. 1–44., 1936.

Kothawala, D. N., Moore, T. R. and Hendershot, W. H.: Soil Properties Controlling the Adsorption of Dissolved Organic Carbon to Mineral Soils, Soil Sci. Soc. Am. J., 73(6), 1831–1842, doi:10.2136/SSSAJ2008.0254, 2009.

Lambert, T., Teodoru, C. R., Nyoni, F. C., Bouillon, S., Darchambeau, F., Massicotte, P. and Borges, A. V: Along-stream transport and transformation of dissolved organic matter in a large tropical river, , (May), 2727–2741, doi:10.5194/bg-13-2727-2016, 2016a.

Lambert, T., Bouillon, S., Darchambeau, F., Massicotte, P. and Borges, A. V: Shift in the chemical composition of dissolved organic matter in the Congo River network, Biogeosciences, 13(18), 5405–5420, doi:10.5194/bg-13-5405-2016, 2016b.

Lauerwald, R., Laruelle, G. G., Hartmann, J., Ciais, P. and Regnier, P. A. G.: Spatial patterns in CO₂ evasion from the global river network, Global Biogeochem. Cycles, 29(5), 534–554, doi:10.1002/2014GB004941, 2015.

Lehner, B., Verdin, K., Jarvis, A. and Systems, E.: New global hydrography derived from spaceborne elevation data, Eos, Trans. Am. Geophys. Union, 89(10), 93–94, 2008.

Lewis, E. and Wallace Upton, N.: Program developed for CO₂ calculations, , doi:10.2172/639712, 1998.

Ludwig, W., Probst, J. and Kempe, S.: Predicting the oceanic input of organic carbon by continental erosion, Global Biogeochem. Cycles, 10(1), 23–41, 1996.

Malard, F. and Hervant, F.: Oxygen supply and the adaptations of animals in groundwater, Freshw. Biol., 41(1), 1–30, doi:10.1046/J.1365-2427.1999.00379.X, 1999.

Maréchal, J., Braun, J., Riotte, J., Bedimo, J. B. and Boeglin, J.: Hydrological processes of a rainforest headwater swamp from natural chemical tracing in Nsimi watershed, Cameroon, Hydrol. Process., 25(14), 2246–2260, 2011.

Mayorga, E., Aufdenkampe, A. K., Masiello, C. A., Krusche, A. V, Hedges, J. I., Quay, P. D., Richey, J. E. and Brown, T. A.: Young organic matter as a source of carbon dioxide outgassing from Amazonian rivers, , doi:10.1038/nature03880, 2005.

Meybeck, M.: Carbon, nitrogen, and phosphorus transport by world rivers, Am. J. Sci., 282(4), 401–450, 1982.

Meybeck, M.: Global chemical weathering of surficial rocks estimated from river dissolved loads, Am. J. Sci., 287(5), 401–428, doi:10.2475/ajs.287.5.401, 1987.

Meybeck, M.: Riverine transport of atmospheric carbon: Sources, global typology and budget, Water, Air, Soil Pollut., 70(1–4), 443–463, doi:10.1007/BF01105015, 1993.

Millero, F. J.: The thermodynamics of the carbonate system in seawater, Geochem. Cosmochem. Ac., 43, 1651–1661, 1979.

Mitsch, W. J., Zhang, L., Stefanik, K. C., Nahlik, A. M., Anderson, C. J., Bernal, B., Hernandez, M. and Song, K.: Creating Wetlands: Primary Succession, Water Quality Changes, and Self-Design over 15 Years, Bioscience, 62(3), 237–250, doi:10.1525/BIO.2012.62.3.5, 2012.

Moore, T. R.: Dissolved organic carbon in a northern boreal landscape, Global Biogeochem. Cycles, 17(4), doi:10.1029/2003GB002050, 2003.

980 Moreira-Turcq, P., Bonnet, M. P., Amorim, M., Bernardes, M., Lagane, C., Maurice, L., Perez, M. and Seyler, P.: Seasonal
 981 variability in concentration, composition, age, and fluxes of particulate organic carbon exchanged between the floodplain and
 982 Amazon River, *Global Biogeochem. Cycles*, 27(1), 119–130, doi:10.1002/gbc.20022, 2013.

983 Moustapha, M., Deirmendjian, L., Sebag, D., Braun, J.-J., Ateba Bessa, H., Adatte, T., Causserand, C., Adamou, I., Ngounou
 984 Ngatcha, B. and Guérin, F.: Data-base for : “Partitioning carbon sources between wetland and well-drained ecosystems to a
 985 tropical first-order stream - Implications to carbon cycling at the watershed scale (Nyong, Cameroon),” ,
 986 doi:10.5281/ZENODO.5625039, 2021.

987 Neff, J. and Asner, G.: Dissolved organic carbon in terrestrial ecosystems: synthesis and a model, *Springer*, 4(1), 29–48,
 988 doi:10.1007/s100210000058, 2001.

989 Nepstad, D. C., Carvalhot, C. R. De, Davidson, E. A., Jipp, P. H., Lefebvre, P. A., Negrelros, G. H., Silvat, E. D., Stone, T. A.
 990 and Trumbore, S. E.: and Pastures, , 372(December), 666–669, 1994.

991 Nkoue-ndondo, G.-R.: Le cycle du carbone en domaine tropical humide: exemple du bassin versant forestier du Nyong au sud
 992 Cameroun, Université de Toulouse, Université Toulouse III-Paul Sabatier., 2008.

993 Nkoue-ndondo, G.-R., Probst, J.-L., Ndjama, J., Ngoupayou, J. R. N., Boeglin, J.-L., Takem, G. E., Brunet, F., Mortatti, J.,
 994 Gauthier-Lafaye, F. and Braun, J.-J.: Stable Carbon Isotopes $\delta^{13}\text{C}$ as a Proxy for Characterizing Carbon Sources and
 995 Processes in a Small Tropical Headwater Catchment: Nsimi, Cameroon, *Aquat. Geochemistry*, 1–30, 2020.

996 Nkoue Ndong, G. R., Probst, J.-L. L., Ndjama, J., Ndam Ngoupayou, J. R., Boeglin, J.-L. L., Takem, G. E., Brunet, F.,
 997 Mortatti, J., Gauthier-Lafaye, F., Braun, J.-J. J., Ekodeck, G. E., Nkoue-ndondo, G.-R., Probst, J.-L. L., Ndjama, J.,
 998 Ngoupayou, J. R. N., Boeglin, J.-L. L., Takem, G. E., Brunet, F., Mortatti, J., Gauthier-Lafaye, F. and Braun, J.-J. J.: Stable
 999 Carbon Isotopes $\delta^{13}\text{C}$ as a Proxy for Characterizing Carbon Sources and Processes in a Small Tropical Headwater Catchment:
 1000 Nsimi, Cameroon, *Aquat. Geochemistry*, 1–30, doi:10.1007/s10498-020-09386-8, 2020.

1001 Nyeck, B., Bilong, P., Monkam, A. and Belinga, S. M. E.: Mise au point d’un modèle de cartographie et de classification des
 1002 sols en zone forestières intertropicales au Cameroun. Cas du plateau forestier humide de Zoétélé, *Géocam2*, Press Uni. Yaoundé,
 1003 171–180, 1999.

1004 Oliva, P., Viers, J., Dupré, B., Fortuné, J., Martin, F., Braun, J., Nahon, D. and Robain, H.: The effect of organic matter on
 1005 chemical weathering: Study of a small tropical watershed: Nsimi-Zoetele site, Cameroon, *Geochim. Cosmochim. Acta*, 63(23–
 1006 24), 4013–4055, 1999.

1007 Olivry, J.: *Fleuves et rivières du Cameroun*, edited by ORSTOM, Paris., 1986.

1008 Peel, M. C., Finlayson, B. L. and McMahon, T. A.: Updated world map of the Köppen-Geiger climate classification, *Hydrol.*
 1009 *Earth Syst. Sci.*, 11(5), 1633–1644, doi:10.5194/hess-11-1633-2007, 2007.

1010 Piedade, M. T. F., Ferreira, C. S., de Oliveira Wittmann, A., Buckeridge, M. and Parolin, P.: Biochemistry of Amazonian
 1011 floodplain trees, in *Amazonian floodplain forests*, pp. 127–139, Springer., 2010.

1012 Raymond, P. A., Zappa, C. J., Butman, D., Bott, T. L., Potter, J., Mulholland, P., Laursen, A. E., McDowell, W. H. and
 1013 Newbold, D.: Scaling the gas transfer velocity and hydraulic geometry in streams and small rivers, *Limnol. Oceanogr. Fluids*

1014 Environ., 2(1), 41–53, doi:10.1215/21573689-1597669, 2012.

1015 Raymond, P. A., Hartmann, J., Lauerwald, R., Sobek, S., McDonald, C., Hoover, M., Butman, D., Striegl, R., Mayorga, E.,
 1016 Humborg, C., Kortelainen, P., Dürr, H., Meybeck, M., Ciais, P. and Guth, P.: Global carbon dioxide emissions from inland
 1017 waters, *Nature*, 503(7476), 355–359, doi:10.1038/nature12760, 2013.

1018 Richey, J. E., Melack, J. M., Aufdenkampe, A. K., Ballester, V. M. and Hess, L. L.: Outgassing from Amazonian rivers and
 1019 wetlands as a large tropical source of atmospheric CO₂, 6416(1991), 6413–6416, 2002.

1020 Sabater, S., Armengol, J., Comas, E., Sabater, F., Urrizalqui, I. and Urrutia, I.: Algal biomass in a disturbed Atlantic river:
 1021 water quality relationships and environmental implications, *Sci. Total Environ.*, 263(1–3), 185–195, doi:10.1016/S0048-
 1022 9697(00)00702-6, 2000.

1023 Sanderman, J. and Amundson, R.: A comparative study of dissolved organic carbon transport and stabilization in California
 1024 forest and grassland soils, *Biogeochemistry*, 89(3), 309–327, doi:10.1007/S10533-008-9221-8, 2008.

1025 Sanders, I. A., Cotton, J., Hildrew, A. G. and Trimmer, M.: Emission of Methane from Chalk Streams Has Potential
 1026 Implications for Agricultural Practices, *Freshw. Biol.*, 52(6), 1176–1186, doi:10.1111/j.1365-2427.2007.01745.x, 2007.

1027 Sauer, D., Sommer, M., Jahn, R., Sauer, D., Sponagel, H., Sommer, M., Giani, L., Jahn, R. and Stahr, K.: Podzol : Soil of the
 1028 Year 2007 . A review on its genesis , occurrence , and functions A review on its genesis , occurrence , and functions, *J. Plant*
 1029 *Nutr. Soil Sci.*, 170(5), 581–597, doi:10.1002/jpln.200700135, 2007.

1030 Saunders, M. J., Jones, M. B. and Kansime, F.: Carbon and water cycles in tropical papyrus wetlands, *Wetl. Ecol. Manag.*,
 1031 15(6), 489–498, doi:10.1007/s11273-007-9051-9, 2007.

1032 Saunio, M., Stavert, A. R., Poulter, B., Bousquet, P., Canadell, J. G., Jackson, R. B., Raymond, P. A., Dlugokencky, E. J.,
 1033 Houweling, S., Patra, P. K., Ciais, P., Arora, V. K., Bastviken, D., Bergamaschi, P., Blake, D. R., Brailsford, G., Bruhwiler,
 1034 L., Carlson, K. M., Carrol, M., Castaldi, S., Chandra, N., Crevoisier, C., Crill, P. M., Covey, K., Curry, C. L., Etiope, G.,
 1035 Frankenberg, C., Gedney, N., Hegglin, M. I., Höglund-Isakson, L., Hugelius, G., Ishizawa, M., Ito, A., Janssens-Maenhout,
 1036 G., Jensen, K. M., Joos, F., Kleinen, T., Krummel, P. B., Langenfelds, R. L., Laruelle, G. G., Liu, L., Machida, T., Maksyutov,
 1037 S., McDonald, K. C., McNorton, J., Miller, P. A., Melton, J. R., Morino, I., Müller, J., Murgia-Flores, F., Naik, V., Niwa, Y.,
 1038 Noce, S., O’Doherty, S., Parker, R. J., Peng, C., Peng, S., Peters, G. P., Prigent, C., Prinn, R., Ramonet, M., Regnier,
 1039 P., Riley, W. J., Rosentreter, J. A., Segers, A., Simpson, I. J., Shi, H., Smith, S. J., Steele, P. L., Thornton, B. F., Tian, H.,
 1040 Tohjima, Y., Tubiello, F. N., Tsuruta, A., Viovy, N., Voulgarakis, A., Weber, T. S., van Weele, M., van der Werf, G. R.,
 1041 Weiss, R. F., Worthy, D., Wunch, D., Yin, Y., Yoshida, Y., Zhang, W., Zhang, Z., Zhao, Y., Zheng, B., Zhu, Q., Zhu, Q. and
 1042 Zhuang, Q.: The Global Methane Budget 2000-2017, *Earth Syst. Sci. Data Discuss.*, 12(3), 1561–1623, doi:10.5194/essd-
 1043 2019-128, 2019.

1044 Sawakuchi, H. O., Neu, V., Ward, N. D., Barros, M. D. L. C., Valerio, A. M., Gagne-Maynard, W., Cunha, A. C., Less, D. F.
 1045 S. S., Diniz, J. E. M., Brito, D. C., Krusche, A. V. and Richey, J. E.: Carbon dioxide emissions along the lower Amazon River,
 1046 *Front. Mar. Sci.*, 4(March), 1–12, doi:10.3389/fmars.2017.00076, 2017.

1047 Schewendenmann, L. and Veldkamp, E.: Long-term CO₂ production from deeply weathered soils of a tropical rain forest:

1048 Evidence for a potential positive feedback to climate warming, *Glob. Chang. Biol.*, 12(10), 1878–1893, doi:10.1111/j.1365-
1049 2486.2006.01235.x, 2006.

1050 Shen, Y., Chapelle, F. H., Strom, E. W. and Benner, R.: Origins and bioavailability of dissolved organic matter in groundwater,
1051 , 61–78, doi:10.1007/s10533-014-0029-4, 2015.

1052 Silva, T. S. F., Melack, J. M. and Novo, E. M. L. M.: Responses of aquatic macrophyte cover and productivity to flooding
1053 variability on the Amazon floodplain, *Glob. Chang. Biol.*, 19(11), 3379–3389, doi:10.1111/GCB.12308, 2013.

1054 Strahler, A. N.: Mtm Quantitative Analysis of Watershed Geomorphology, *Trans. Am. Geophys. Union*, 38(6), 913–920, 1957.

1055 Suchel, J.-B.: Les climats du Cameroun, Université de Bordeaux III, France., 1987.

1056 Tamoooh, F., Van Den Meersche, K., Meysman, F., Marwick, T. R., Borges, A. V, Merckx, R., Dehairs, F., Schmidt, S., Nyunja,
1057 J. and Bouillon, S.: Distribution and origin of suspended matter and organic carbon pools in the Tana River Basin, Kenya,
1058 *Biogeosciences*, 9(8), 2905–2920, doi:10.5194/bg-9-2905-2012, 2012.

1059 Tamoooh, F., Meysman, F. J. R., Borges, A. V, Marwick, T. R., Van, K., Meersche, D., Dehairs, F., Merckx, R. and Bouillon,
1060 S.: Sediment and carbon fluxes along a longitudinal gradient in the lower Tana River (Kenya), *Biogeosciences*, 11(7), 1340–
1061 1353, doi:10.1002/2013JG002358, 2014.

1062 Tank, J. L., Baker, M. A., Hotchkiss, E. R. and Rosi-marshall, E. J.: Metabolism , Gas Exchange , and Carbon Spiraling in
1063 Rivers, , 2016, 73–86, 2016.

1064 Tsy-pin, M. and Macpherson, G. L.: The effect of precipitation events on inorganic carbon in soil and shallow groundwater,
1065 Konza Prairie LTER Site, NE Kansas, USA, *Appl. geochemistry*, 27(12), 2356–2369, 2012.

1066 Viers, J., Dupré, B., Polvé, M., Schott, J., Dandurand, J. L. and Braun, J. J.: Chemical weathering in the drainage basin of a
1067 tropical watershed (Nsimi-Zoetele site, Cameroon) : comparison between organic-poor and organic-rich waters, *Chem. Geol.*,
1068 140(3–4), 181–206, doi:10.1016/S0009-2541(97)00048-X, 1997.

1069 Viers, J., Dupré, B., Braun, J. J., Deberdt, S., Angeletti, B., Ngoupayou, J. N. and Michard, A.: Major and trace element
1070 abundances, and strontium isotopes in the Nyong basin rivers (Cameroon): constraints on chemical weathering processes and
1071 elements transport mechanisms in humid tropical environments, *Chem. Geol.*, 169(1–2), 211–241, doi:10.1016/S0009-
1072 2541(00)00298-9, 2000.

1073 Weiss, R. F.: Carbon dioxide in water and seawater: the solubility of a non-ideal gas, *Mar. Chem.*, doi:10.1016/0304-
1074 4203(74)90015-2, 1974.

1075 White, A. F. and Blum, A. E.: Effects of climate on chemical_ weathering in watersheds, *Geochim. Cosmochim. Acta*, 59(9),
1076 1729–1747, 1995.

1077

Table 1: Geographical and hydrological sub-catchments characteristics. ^a represents Q_{hill} (Fig. 3) and it is estimated from equation 1.

Rivers	<i>Mengong</i>	<i>Mengong</i>	<i>Awout</i>	<i>So'o</i>	<i>Nyong</i>	<i>Nyong</i>
Stations	Source	Outlet	Messam	Pont So'o	Mbalmayo	Olama
Latitude	3.17°N	3.17°N	3.28°N	3.32°N	3.52°N	3.43°N
Longitude	11.83°E	11.83°E	11.78°E	11.48° E	11.5°E	11.28°E
Gauging station	No	Yes	Yes	Yes	Yes	Yes
Altitude (m)	680	669	647	634	634	628
Catchment area (km²)	0.48	0.6	206	3 070	13 555	18 510
Wetlands (%)		20	5.7	5.3	4.6	4.4
Catchment slope (‰)	1.3	1.3	1.2	1.1	0.16	0.15
Stream order	groundwater	1	3	4	5	6
Averaged-annual river flow in 2016 (m ³ s ⁻¹)	0.00544 ^a	0.009±0.002	3.9±4.8	35.6±40.6	146±112	195±160
Averaged-annual rainfall (mm yr ⁻¹)	1 986					

1080

Table 2: Spatial distribution of physicochemical parameters (yearly average±standard deviation) in waters of the Nyong watershed during the sampling year 2016. The range is shown in square brackets. ^a was measured in the topsoil solution of the Mengong wetland at 0.4 m depth by Nkoue-Ndondo et al. (2020).

Parameters	T	pH	Specific conductivity	Oxygen saturation	TSM
Units	°C	Unitless	µS cm ⁻¹	%	mg L ⁻¹
Mengong wetland ^a	24.2±1.4	5.5±0.6			
	[21.9-26.3]	[4.9-6.6]			
Mengong source	23.2±0.1	5.0±0.1	15.1±0.8	50±8	
	[23~23.6]	[4.6~5.3]	[14.1~17.4]	[38~68]	
Mengong outlet (order 1)	22.9±0.7	5.6±0.2	16.7±4.5	52±7	5.3±2.1
	[21.9~24.4]	[5.3~6.0]	[5.2~24.7]	[39~62]	[1.8~11.1]
Awout (order 3)	22.5±0.5	5.6±0.2	21.6±5.5	47±9	10.4±6.1
	[22~23.5]	[5.0~6.1]	[16.5~40.3]	[37~67]	[4.9~27.5]
So'o (order 4)	23.9±1.3	6.1±0.2	23.4±5.0	57±6	14.4±3.8
	[22.4~27.6]	[5.7~6.6]	[18.3~35]	[46~69]	[8.2~22.9]
Nyong (Mbalamayo, order 5)	26.1±1.3	6.2±0.3	36.6±19	40±20	8.9±2.0
	[24.3~29.0]	[5.5~6.9]	[19.6~86.3]	[13~81]	[4.3~12.0]
Nyong (Olama, order 6)	25.7±1.4	6.2±0.3	31.4±12.8	43±12	9.7±3.2
	[24.1~28.8]	[5.5~6.6]	[20.1~69.3]	[24~67]	[3.7~14.8]

Table 3: Spatial distribution of C variables (yearly average±standard deviation) in waters of the Nyong watershed during the sampling year 2016. The range is shown in square brackets. ^ameasured in the topsoil solution of the Mengong wetland at 0.4 m depth by Nkoue-Ndondo et al. (2020). ^b measured in the topsoil solution of the Mengong wetland at 0.4 m depth by Braun et al. (2005).

Parameters	pCO ₂	TA	DIC	DOC	POC	POC
Units	ppmv	μmol L ⁻¹	μmol L ⁻¹	μmol L ⁻¹	%	μmol L ⁻¹
Mengong wetland	36 840±23 190 ^a [3 900-84 240]	122±46 ^a [50-216]	1 430±900 ^a [150-3 270]	1 420±750 ^b [1 250 - 2 920]		
Mengong source	78 800±40 110 [12 700~209 000]	53±26 [15~138]	2 940±1 485 [500~7 560]	83		
Mengong outlet (order 1)	15 600±8 900 [3 980~41 000]	90± 36 [20~156]	670±360 [170~1 710]	1 925±970 [1 090~4 150]	23±5 [14~26]	101±44 [14~213]
Awout (order 3)	15 400±7 300 [5 760~26 710]	67±39 [11~166]	670±315 [260~1 170]	3 200±1 840 [2 000~7 550]	16±3 [11~21]	130±50 [72~243]
So'o (order 4)	12 700±5 100 [4 900~23 200]	74±34 [10~145]	670±260 [300~1 320]	2 170±980 [1 100~5 320]	18±4 [12~29]	210±60 [125~360]
Nyong (Mbalamayo, order 5)	11 800±5 100 [3 620~22 460]	123±63 [20~230]	720±270 [220~1 200]	2 000±860 [1 020~5 300]	20±3 [16~26]	150±40 [62~220]
Nyong (Olama, order 6)	11 000±5 550 [3 000~21 700]	134±70 [10~265]	640±330 [170~1 240]	1 860±440 [1 100~2 880]	18±2 [15~23]	150±50 [55~235]

1100 **Table 4: Correlations (Pearson’s Correlation test) between C or ancillary parameters and the discharge in**
the different stream orders. The Pearson’s Correlation coefficient is indicated and significant correlations
(p<0.05) are in bold.

1105

	Mengong	Awout	So'o	Nyong at Mbalmayo	Nyong at Olama	
	Discharge	Discharge	Discharge	Discharge	Discharge	
Oxygen saturation	0.19	-0.32	-0.54	-0.85	-0.85	
pH	-0.60	-0.17	-0.53	-0.76	-0.81	1110
Specific conductivity	-0.02	0.11	-0.44	-0.63	-0.70	
TA	0.21	0.21	-0.39	-0.41	-0.37	
pCO ₂	0.05	0.32	-0.03	0.46	0.38	
DOC	0.32	-0.15	0.14	-0.14	0.28	
TSM	-0.28	-0.56	-0.32	0.33	0.56	1115
POC%	-0.50	-0.22	0.36	0.62	0.38	
POC	-0.43	-0.62	0.27	0.46	0.70	

1120 **Table 5: DOC, DIC and POC budgets in the first-order Mengong stream (Eqs. 8-10). Fluxes are in MgC yr^{-1} and are described in details in the section 2.5. Briefly, F_{GW} is the quantity of dissolved carbon leached from non-flooded forest groundwater to the Mengong stream (Eq. 11), F_{WL} is the quantity of carbon leached from the Mengong wetland to the Mengong stream (Eqs. 13-14), F_{D} is the quantity of CO_2 degassed from the Mengong stream to the atmosphere, F_{RH} is the heterotrophic respiration in the Mengong stream, and F_{OUT} is the quantity of carbon hydrologically exported at the outlet of the Mengong stream.**

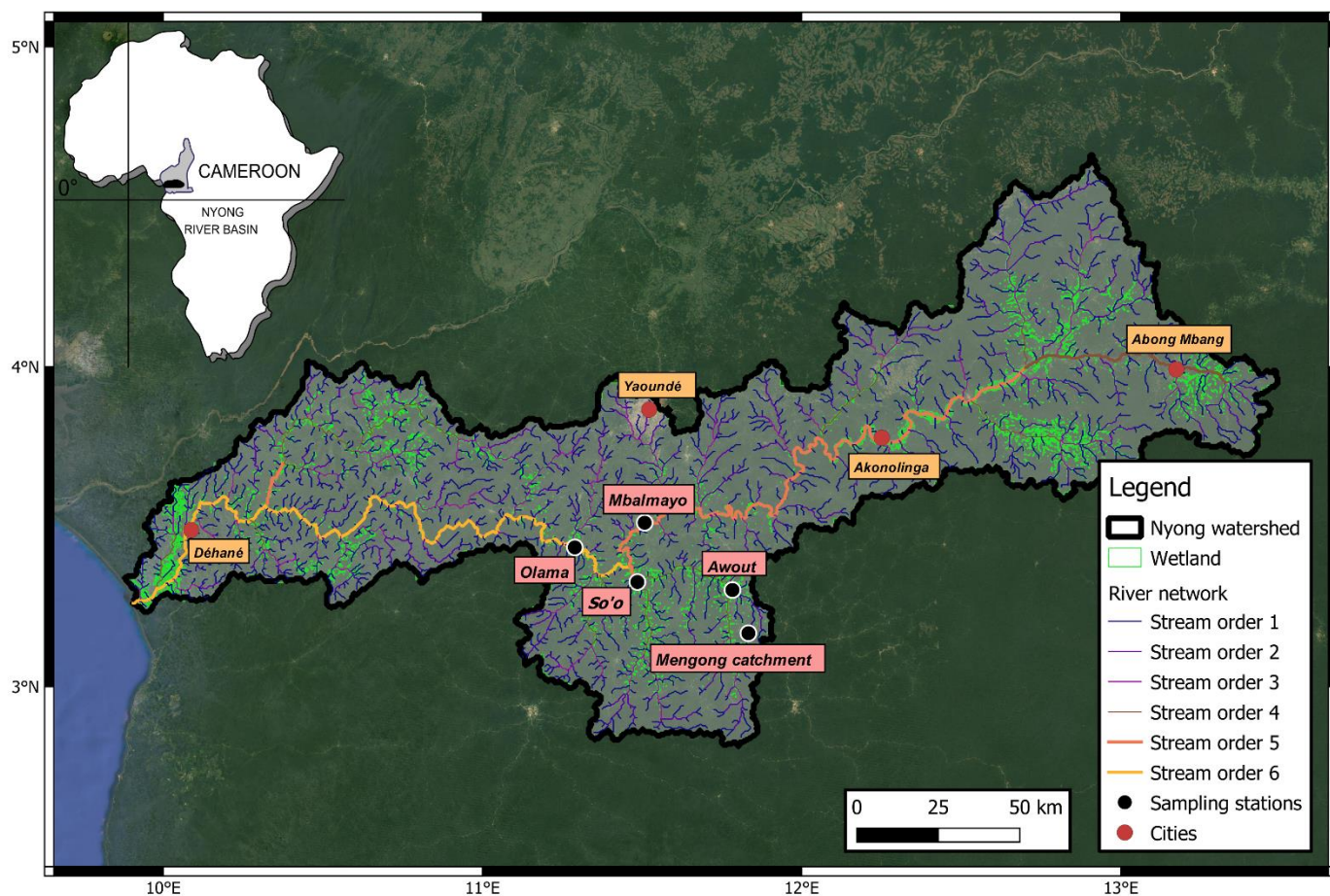
1125		DOC _{budget}	DIC _{budget}	POC _{budget}
	F_{GW}	0.17±0.02	6.05±2.98	
	F_{WL}	1.80±0.95	1.82±1.13	0.34±0.14
	F_{D}		5.51±2.30	
	F_{RH}	0.32±0.30	0.32±0.30	
1130	F_{OUT}	6.41±3.23	2.23±1.20	0.34±0.14
	Imbalance (inputs-outputs)	-4.76	0.45	0

Stream order	Respiration rates gC-CO ₂ m ⁻² yr ⁻¹	<i>k</i> ₆₀₀ m d ⁻¹	F _{degas} gC-CO ₂ m ⁻² yr ⁻¹	Water surface area m ²	F _{degas} GgC-CO ₂ yr ⁻¹
1	63.9±49.2 (286.4±227.9 ^a)	2.21±0.08 [2.04-2.31] 2.58±0.19	5 344±2 773 [2 436-12 089]	6 662±3340 [337-11 5950]	42.5±26.7 [14.2-100.3] 126.5±60.2
2		[2.18-2.83] 2.94±0.29	[2 936-10 739]	[2 794-27 216]	[49.8-220.9] 137.0±57.0
3		[2.46-3.33] 3.00±0.31	[3 155-10 800]	[5 728-27 538]	[61.4-228.7] 114.4±79.9
4		[2.55-3.45] 2.35±0.10	[363- 9 997]	[8117-34 143]	[3.9-318.7] 90.3±58.0
5	533.4±534.3 (755.9±333.0 ^a)	[2.20-2.51] 2.48±0.13	[1 114-6 230]	[9 656-40 207]	[19.8-222.2] 141.3±92.0
6		[2.28-2.71]	[957-6 354]	[15 741-65 121]	[35.9-317.8] 651.9±160.6 ^b (23.4±5.8 ^c)

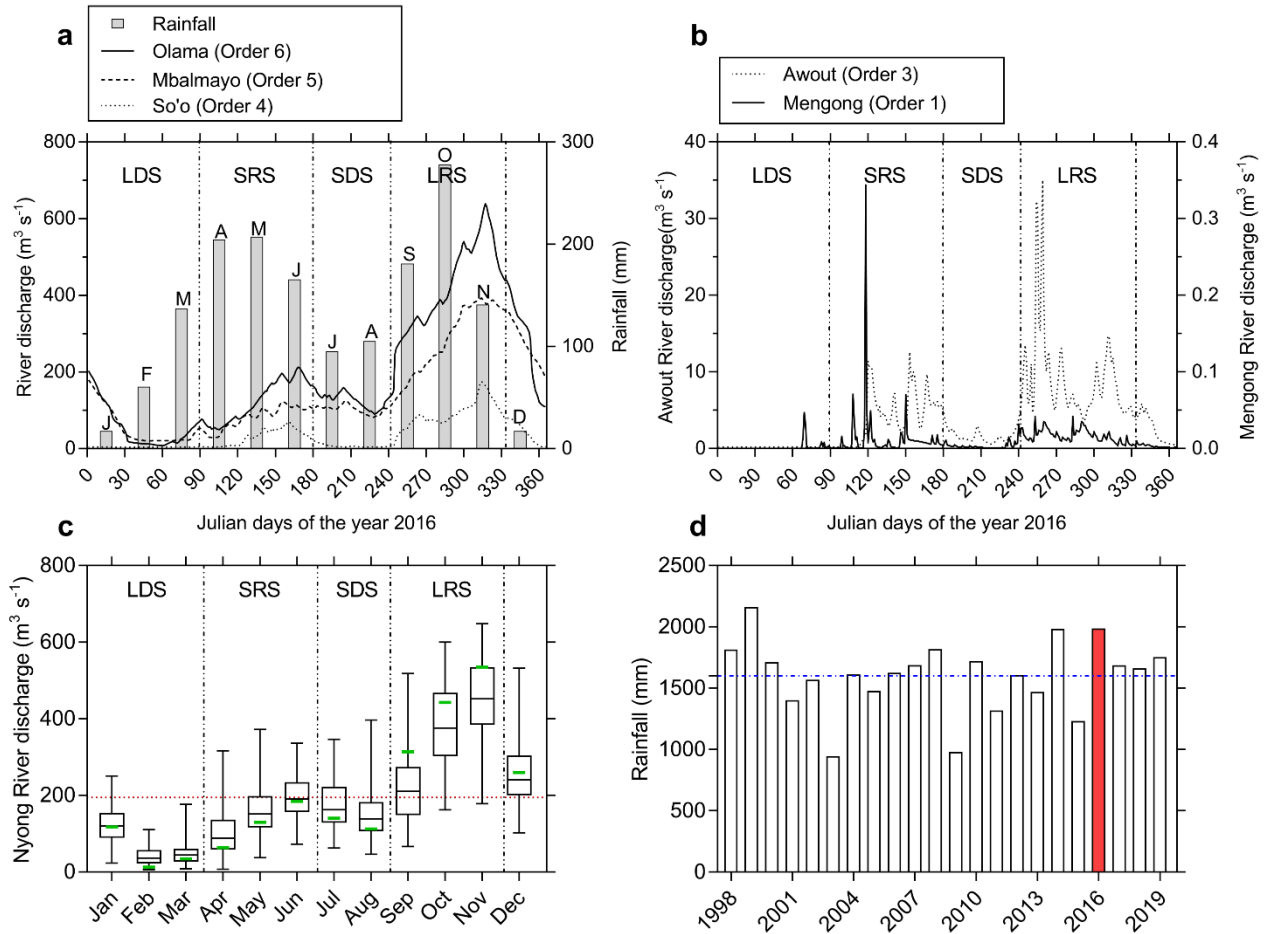
Table 6: At the Nyong watershed scale, yearly averages with standard deviations (based on averaging monthly values in each stream order) of CO₂ degassing rates (F_{degas} in gC-CO₂ m⁻² yr⁻¹), *k*₆₀₀ (m d⁻¹), water surface area (m²), and integrated CO₂ degassing flux (F_{degas} in GgC-CO₂ yr⁻¹), estimated in the different stream orders. Range (based on monthly values) is shown between brackets. In addition, rates of heterotrophic respiration (gC-CO₂ m⁻² yr⁻¹) in the stream orders 1 and 5 are indicated. ^a considering an additional benthic respiration in tropical rivers of 222 gC m⁻² yr⁻¹ by Cardoso et al. (2014). ^b calculated as the sum of the integrated CO₂ degassing flux in each stream order, this represents the CO₂ degassing flux from the entire river network (GgC-CO₂ yr⁻¹). ^c this represents the CO₂ degassing flux from the entire river network weighed by the surface area of the Nyong watershed (MgC-CO₂ km⁻² yr⁻¹). Note that measurements in second-order streams were extrapolated (see method).

1150 **Table 7: At the Nyong watershed scale, averages of monthly hydrological export of C to the ocean (F_{ocean}) and of monthly CO₂ degassing to the atmosphere (F_{degas}). ^a the net C sink estimated by Brunet et al. (2009) for the entire Nyong watershed is also indicated.**

	F_{ocean} GgC yr ⁻¹	F_{degas} GgC-CO ₂ yr ⁻¹	F_{ocean} MgC km ⁻² yr ⁻¹	F_{degas} MgC-CO ₂ km ⁻² yr ⁻¹	Watershed net C sink ^a MgC km ⁻² yr ⁻¹
DOC	134.0±99.8		7.2±5.		
DIC	45.5±42.4	651.9±160.6	2.4±2.3	23.4±5.8	
POC	11.9±9.9		0.6±0.5		
					1155
Total	191.4±108.9	651.9±160.6	10.3±5.8	23.4±5.8	300
					1160



1165 **Figure 1: Map of the Nyong watershed showing the river network, the wetland extent from Gumbricht et al. (2017) and the location of the sampling stations and some cities. Note, the Nyong River is displayed bolder than the other rivers. The background map is from Google Satellite®.**



1170 **Figure 2: (a-b) River discharges of the different gauging stations during the sampling year 2016, associated**
with rainfall measured at the Mengong catchment. (c) The box plots represent the variability of monthly
Nyong River discharges from 1998 to 2020 and extreme box plots values represent minimum and maximum
monthly discharges during the same period; whereas the green lines represent the average monthly
discharges in 2016, and the red dashed line represents the yearly average discharge of $194.5 \text{ m}^3 \text{s}^{-1}$ for the
1175 **1998 to 2020 period (very close to the yearly average discharge of $195 \text{ m}^3 \text{s}^{-1}$ measured in 2016). (d) Yearly**
rainfall in the Nyong watershed (measured in the Mengong catchment); the blue line represents the mean
rainfall over the 1998-2020 period ($1600 \pm 290 \text{ mm}$), and the red bar represents the yearly rainfall during the
sampling year 2016. Hydrologic and rainfall data are from Audry et al. (2021).

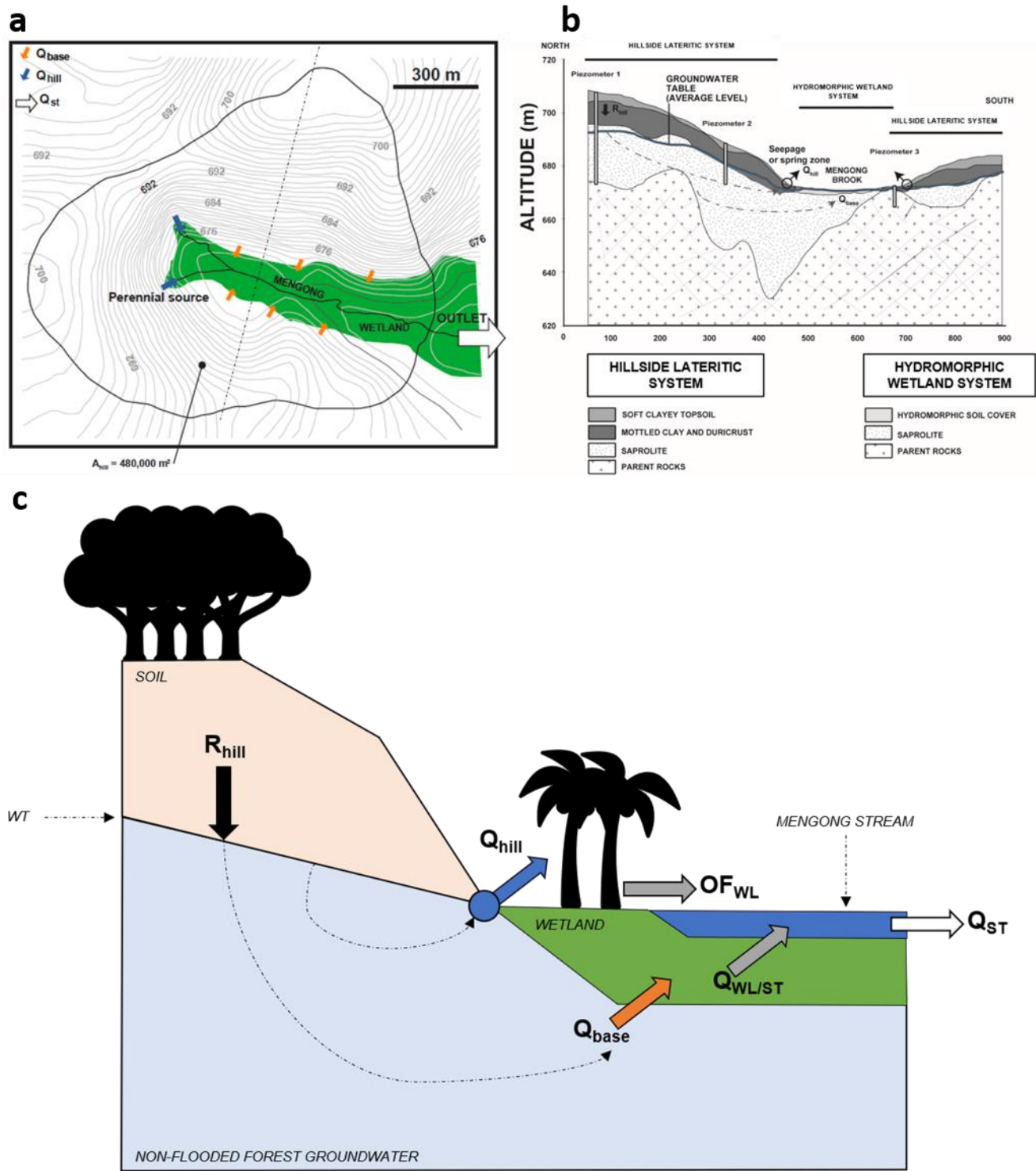


Figure 3: (a) Map of the first-order Mengong catchment showing the wetland area and the hydrological fluxes that are partitioned between the main perennial source (Q_{hill} , blue arrows) of the non-flooded forest groundwater, specific seepage points all around the hillside/wetland boundaries (Q_{base} , orange arrows) of the non-flooded forest groundwater, and the discharge at the stream outlet (Q_{st} , white arrow). Note, A_{hill} is the surface area drained by the non-flooded forest groundwater. (b) Cross section of the dashed line from the map (a), showing the lithology of the hillside lateritic system and the hydromorphic wetland system, the recharge of the hillside system (R_{hill}); Q_{base} and Q_{hill} are also indicated. (c) Hydrological functioning of the first-order Mengong catchment. Note, $Q_{\text{WL/ST}}$ represents the groundwater flow exchanged between the wetland and the stream and OF_{WL} is the overland flow on the surface of the wetland. The figure 3 was adapted from Braun et al. (2005) and (2012) and from Maréchal et al. (2011).

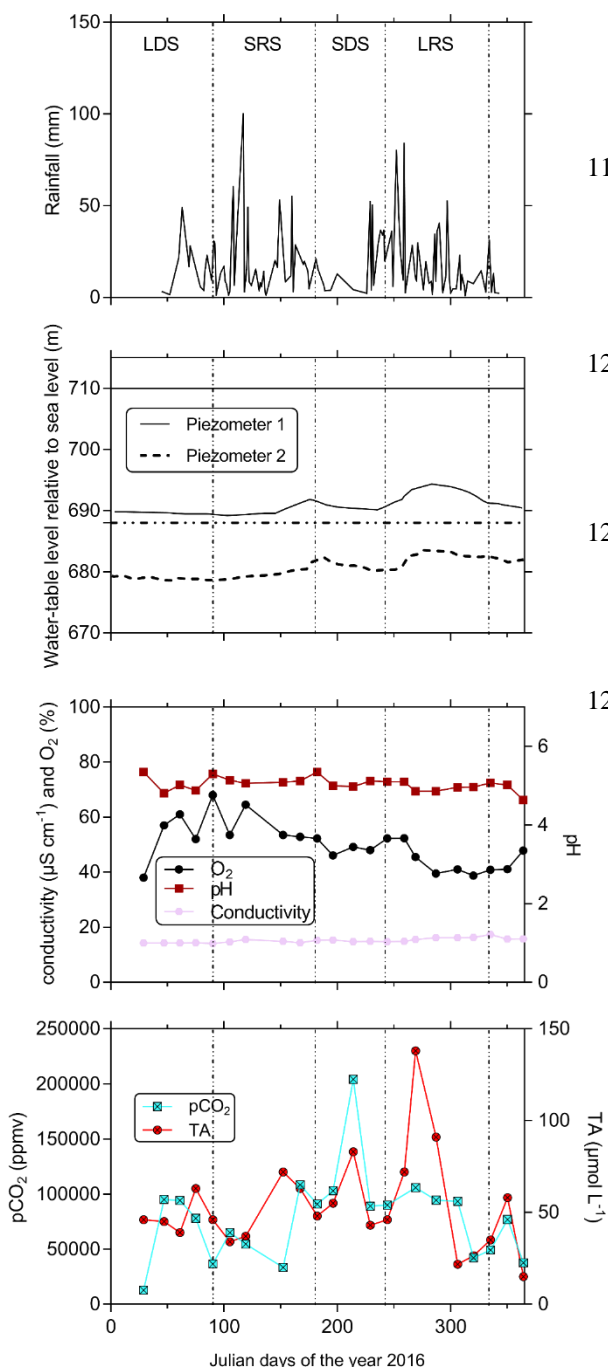
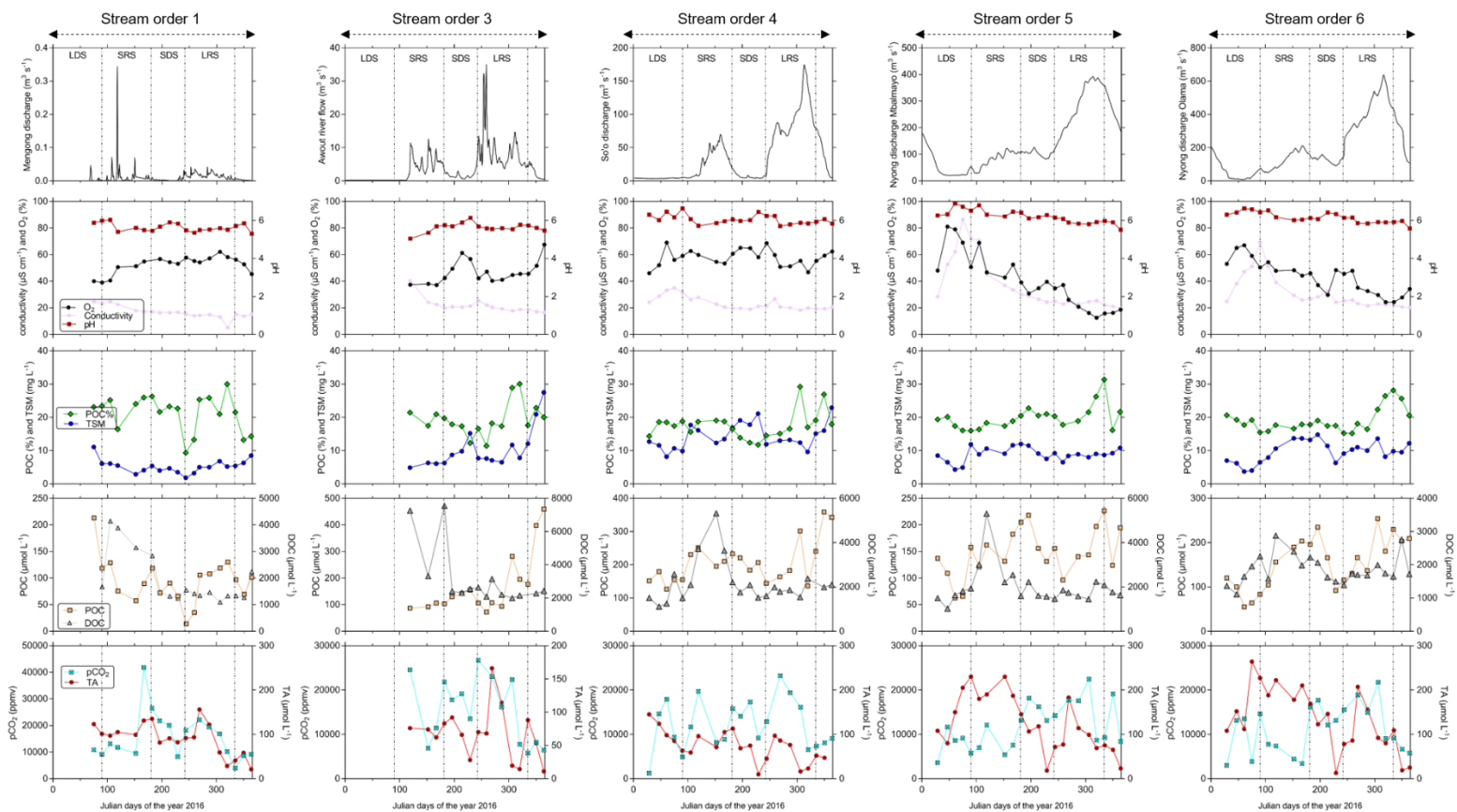


Figure 4: In the first-order Mengong catchment temporal variations of rainfall, water-table level in piezometer 1 and 2 (see figure 3b) relative to sea level (elevation of the soil surface at piezometers 1 and 2 relative to sea level is also indicated by the horizontal lines); and pCO_2 , TA and ancillary parameters (oxygen saturation as O_2 , pH, conductivity as specific conductivity) in non-flooded forest groundwater (measured at the perennial source). The temporal variations are separated into the four seasons that occurs in the Nyong watershed that are LDS as long dry season, SRS as short rainy season SDS as short dry season and LRS as long rainy season. Note, groundwater table level was retrieved from Nkoue-ndondo et al. (2020).



1215 **Figure 5: temporal variations of river discharge, carbon (pCO₂, TA, DOC, POC) and ancillary parameters (oxygen saturation as O₂, pH, conductivity as specific conductivity, TSM) in surface waters of the Nyong watershed. The temporal variations are separated into the four seasons that occurs in the Nyong watershed that are LDS as long dry season, SRS as short rainy season SDS as short dry season and LRS as long rainy season.**

1220

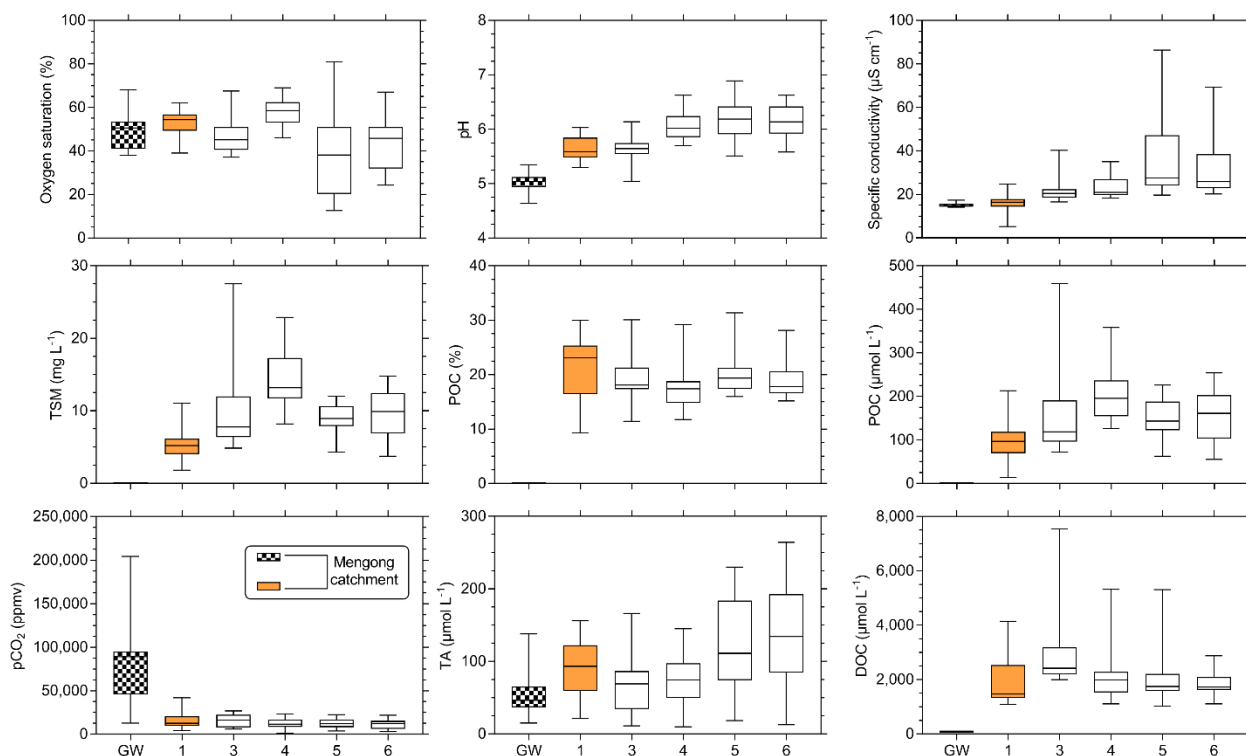


Figure 6: spatial variations of carbon parameters (pCO₂, TA, DOC, POC) and ancillary parameters (oxygen saturation, pH, specific conductivity, TSM) across non-flooded forest groundwater (GW) and streams orders 1, 3, 4, 5 and 6 in the Nyong watershed. Note that the hashed and orange boxplots are for non-flooded forest groundwater and first-order stream, respectively. The boxplots represent the minimum, the first quartile, the median, the third quartile and the maximum.

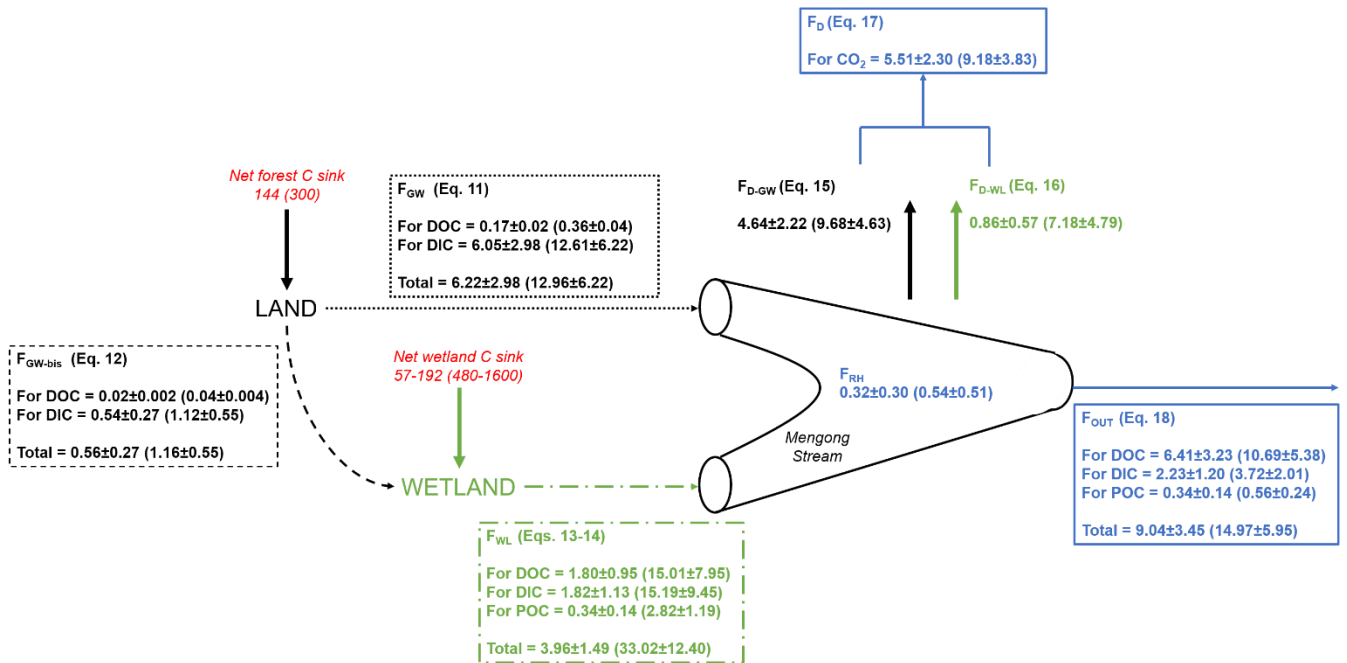


Figure 7: mass balance of C in the first-order Mengong catchment. All fluxes are in $MgC\ yr^{-1}$, and in $MgC\ km^{-2}\ yr^{-1}$ when between brackets (weighed by the surface area of $0.48\ km^2$ drained by non-flooded forest groundwater for the net forest C sink, F_{GW} , F_{GW-bis} and F_{D-GW} , by the wetland surface area of $0.12\ km^2$ for the net wetland C sink, F_{WT} and F_{D-W} , and by the Mengong catchment area of $0.6\ km^2$ for F_{OUT} , F_D and F_{RH}), and they are associated with their corresponding equations as described in details in the section 2.5. Briefly, F_{GW} is the quantity of dissolved carbon leached from non-flooded forest groundwater to the Mengong stream (Eq. 11), F_{GW-bis} is the quantity of dissolved carbon leached from non-flooded forest groundwater to the Mengong wetland (Eq. 12), F_{WL} is the quantity of carbon leached from the Mengong wetland to the Mengong stream (Eqs. 13-14), F_D is the quantity of C degassed from the Mengong stream to the atmosphere, F_{RH} is the heterotrophic respiration in the Mengong stream, and F_{OUT} is quantity of carbon hydrologically exported at the outlet of the Mengong stream. In addition, net forest C sink of the Mengong catchment estimated by Brunet et al. (2009), and a range of typical net wetland C sink measured in wetlands in Africa by Saunders et al. (2007) and Jones and Humphries (2002) are both indicated.

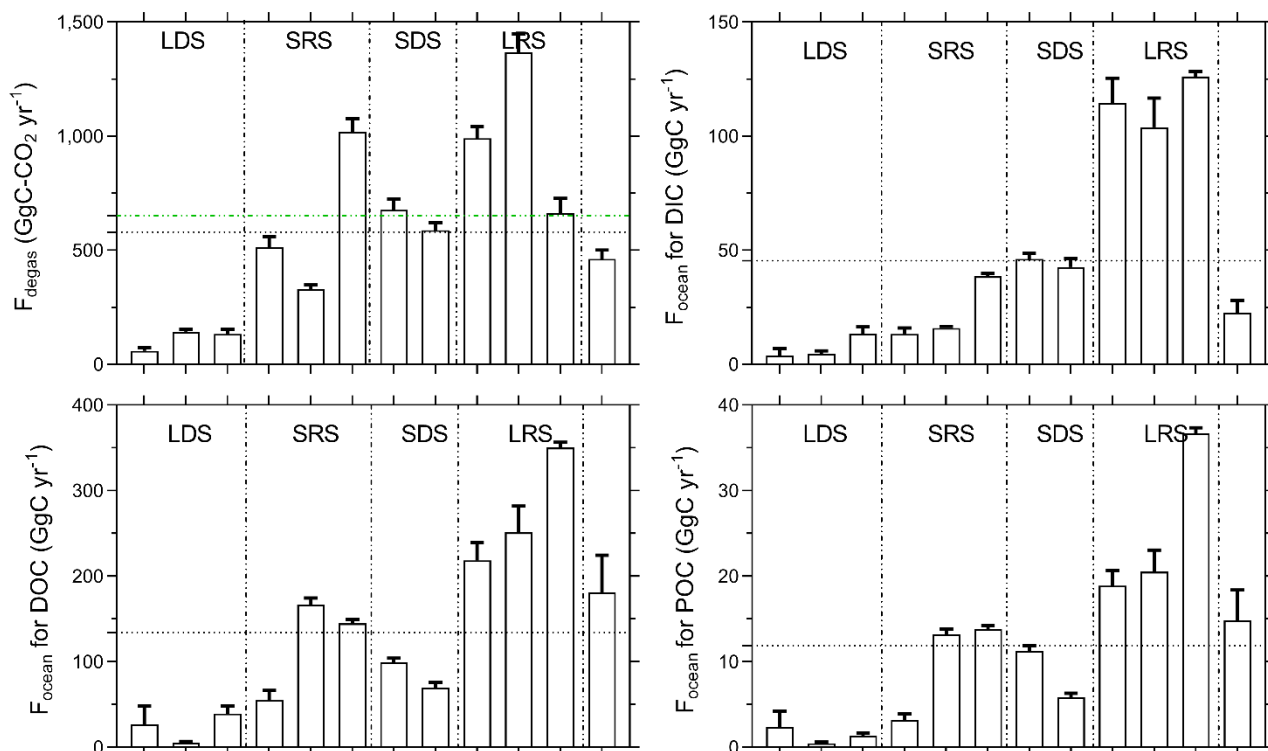


Figure 8: Monthly C fluxes at the Nyong watershed scale described in the section 2.4. For F_{ocean} , the black dashed lines represent the yearly average of the different monthly C fluxes. For F_{degas} , the green dashed line is obtained by summing yearly integrated CO₂ deassing in each stream order, as in Table 6, which represents 651.9±160.6 GgC yr⁻¹. For F_{degas} , the black dashed line represents the yearly average of the different monthly CO₂ degassing fluxes from the entire river network, as in Figure 8, which represents 578.9±157.9 GgC yr⁻¹. The figures are separated into the four seasons that occurs in the Nyong watershed that are LDS as long dry season, SRS as short rainy season SDS as short dry season and LRS as long rainy season.

